

Universality of nucleon-nucleon short-range correlations: the factorization property of the nuclear wave function, the relative and center-of-mass momentum distributions, and the nuclear contacts

M. Alvioli^{1*,†}, C. Ciofi degli Atti^{2,‡} and H. Morita^{3§}

¹CNR-IRPI, Istituto di Ricerca per la Protezione Idrogeologica, Via Madonna Alta 126, I-06128, Perugia, Italy

²Istituto Nazionale di Fisica Nucleare, Sezione di Perugia,

Department of Physics, University of Perugia, Via A. Pascoli, I-06123, Italy

³Sapporo Gakuin University, Bunkyo-dai 11, Ebetsu 069-8555, Hokkaido, Japan

(Dated: July 15, 2016)

Background: the two-nucleon momentum distributions of nucleons N_1 and N_2 in a nucleus A , $n_A^{N_1 N_2}(\mathbf{k}_{rel}, \mathbf{K}_{c.m.})$, is a relevant quantity that determines the probability to find the two nucleons with relative momentum \mathbf{k}_{rel} and center-of-mass (c.m.) momentum $\mathbf{K}_{c.m.}$; at large values of the relative momentum and, at the same time, small values of the c.m. momentum, $n_A^{N_1 N_2}(\mathbf{k}_{rel}, \mathbf{K}_{c.m.})$ provides information on the short-range structure of nuclei.

Purpose: calculation of the momentum distributions of proton-neutron and proton-proton pairs in ^3He , ^4He , ^{12}C , ^{16}O and ^{40}Ca , in correspondence of various values of \mathbf{k}_{rel} and $\mathbf{K}_{c.m.}$.

Methods: the momentum distributions for $A > 4$ nuclei are calculated as a function of the relative, k_{rel} , and center of mass, $K_{c.m.}$, momenta and relative angle Θ , within a linked cluster many-body expansion approach, based upon realistic local two-nucleon interaction of the Argonne family and variational wave functions featuring central, tensor and spin-isospin correlations.

Results: independently of the mass number A , at values of the relative momentum $k_{rel} \gtrsim 1.5 \sim 2 fm^{-1}$ the momentum distributions exhibit the property of factorization, $n_A^{N_1 N_2}(\mathbf{k}_{rel}, \mathbf{K}_{c.m.}) \simeq n_{rel}^{N_1 N_2}(k_{rel}) n_{c.m.}^{N_1 N_2}(K_{c.m.})$, in particular for pn back-to-back (BB) pairs one has $n_A^{pn}(k_{rel}, K_{c.m.} = 0) \simeq C_A^{pn} n_D(k_{rel}) n_{c.m.}^{pn}(K_{c.m.} = 0)$ where n_D is the deuteron momentum distribution, $n_{c.m.}^{pn}(K_{c.m.} = 0)$ the c.m. motion momentum distribution of the pair and C_A^{pn} the pn nuclear contact measuring the number of BB pn pairs with deuteron-like momenta ($\mathbf{k}_p \simeq -\mathbf{k}_n, \mathbf{K}_{c.m.} = 0$). The values of the pn nuclear contact are extracted from the general properties of the two-nucleon momentum distributions corresponding to $K_{c.m.} = 0$. The $K_{c.m.}$ -integrated pn momentum distributions exhibit the property $n_A^{pn}(k_{rel}) \simeq C_A^{pn} n_D(k_{rel})$ but only at very high value of $k_{rel} \gtrsim 3.5 \sim 4 fm^{-1}$. The theoretical ratio of the pp/pn momentum distributions of ^4He and ^{12}C and the calculated c.m. motion momentum distributions are in agreement with recent experimental data.

PACS numbers: 21.30.Fe, 21.60.-n, 24.10.Cn, 25.30.-c

I. AIM AND INTRODUCTION

The investigation of short-range correlations (SRCs) in nuclei is ultimately aimed at unveiling the details of in-medium short-range nucleon-nucleon (NN) dynamics, a relevant physics issue that cannot be answered by scattering experiments of two free nucleons (see recent review papers on the subject [1–5]). A reliable way to gather information on SRCs would be to detect significant deviations of proper experimental data (e.g. electrodisintegration processes off nuclei) from theoretical predictions based upon *ab initio* solutions of the nuclear many-body problem, obtained from various NN interactions differing in the short-range part. In practice such an approach faces several problems because it implies the ex-

act calculation of the ground- and continuum-state wave functions of the target nucleus under investigation; concerning the former, relevant progress has recently been made to obtain *ab initio* solutions of the non relativistic Schrödinger equation, but, unfortunately, the treatment of the continuum spectrum of the target nucleus is still model-dependent, with the only exception of those processes involving the two- and three-nucleon systems; for complex nuclei approximations are unavoidable, with the simplest one being the plane wave impulse approximation (PWIA) which leads, in the case of, e. g., a process $A(e, e'N)X$, to a factorized cross sections depending upon the elementary electron-nucleon cross section and the one-nucleon spectral function $P_A(E, k)$ which describes the momentum ($k \equiv |\mathbf{k}|$) and removal energy (E) distributions of a nucleon in nucleus A (in a process $A(e, e'N_1 N_2)X$) the factorized cross section will depend upon the two-nucleon spectral function, etc.). Even if the PWIA requires corrections due to the final state interaction (FSI) and possible effects from non-nucleonic degrees of freedom, the detection of high momentum and high removal energy effects may represents evidence of ground-state SRCs. It is for this reason that during the last few years, the calculation of the nuclear momentum distri-

*Supported by grants provided by the Regione Umbria, under contract POR-FESR Umbria 20072013, asse ii, attività a1, azione 5, and by the Dipartimento della Protezione Civile, Italy.

†Electronic address: massimiliano.alvioli@irpi.cnr.it

‡Electronic address: ciofi@pg.infn.it

§Electronic address: hiko@webmail.sgu.ac.jp

butions and spectral function has attracted an increasing interest. The one-nucleon, $n_A(k_1)$, and two-nucleon, $n_A(\mathbf{k}_1, \mathbf{k}_2)$, momentum distributions of few-nucleon systems ($A \leq 4$) have been obtained *ab initio* [6–10] within different theoretical approaches and using realistic NN interactions, whereas for $A \leq 12$ exact variational Monte Carlo (VMC) calculations have recently been performed [11]. For nuclei with $A > 12$, VMC calculations of the momentum distribution are not yet feasible, therefore, also in light of future experimental developments, alternative approaches, even if of lower quality than VMC ones, but still maintaining a realistic link to the underlying NN interactions, should be pursued. A serious candidate in this respect would be an advanced linked cluster expansion approach with correlated wave functions, including a large class of Yvon-Mayer diagrams [12–14], for they have been shown to produce realistic results of one-nucleon momentum distributions [15–17] in reasonable agreement with the more advanced VMC calculations. All of these calculations, though being performed within different many-body approaches, produce similar results demonstrating a universal (A-independent) character of in-medium NN short-range dynamics, in that the mean-field (MF) approach breaks down when the relative distance $r \equiv |\mathbf{r}_1 - \mathbf{r}_2|$ between two generic nucleons "1" and "2" is of the order of $r \lesssim 1.3 - 1.5$ fm, with the two-nucleon density distribution exhibiting the so called *correlation hole* which, apart from trivial normalization factors, turns out to be independent on the mass A of the nucleus and similar to the deuteron one. SRCs give rise to high momentum components that are lacking in a mean-field approach and turned out to depend upon the relative orbital momentum (L) and the total spin (S) and isospin (T) of the NN pair, as well as upon the value of the pair center-of-mass (c.m.) momentum. SRCs give rise to peculiar configurations of the nuclear wave function in momentum space, e.g. the ones when a high momentum nucleon is mostly balanced by another nucleon with similar and opposite value of the momentum (the *back-to-back* (BB) configuration) and not by the $A - 1$ nucleon, as in the case of a mean-field configuration [18]. Thus, within a PWIA picture, if a correlated nucleon, with momentum \mathbf{k}_1 , acquiring a momentum \mathbf{q} from an external probe, leaves the nucleus without any final-state interaction (FSI) and is detected with momentum $\mathbf{p} = \mathbf{k}_1 + \mathbf{q}$, the partner nucleon should be emitted with momentum $\mathbf{k}_2 \simeq \mathbf{p}_m = -\mathbf{k}_1$, where the measurable momentum \mathbf{p}_m is the *missing momentum* $\mathbf{p}_m = \mathbf{q} - \mathbf{p}$. Such a basic picture of *back-to-back* short-range correlated (SRCd) nucleons has been recently improved to a large extent by taking into account the FSI of the struck nucleon by advanced methods (see *e.g.* Refs. [19, 20] and [21, 22]) and by considering the effects due to the center-of-mass motion of the pair, which makes $\mathbf{k}_2 \neq -\mathbf{k}_1$, and the effects due to the (ST) dependence. The underlying dynamics of SRCs has been theoretically explained by advanced many-body theories, *e.g.* by the Brueckner-Bethe-Goldstone approach for nuclear matter [23] and by

exact few-nucleon approaches in case of ^3He and ^4He [24], with both approaches demonstrating that two-nucleon correlations arise from a general property of the many-body wave function, namely its factorized form in those configurations where a pair of nucleons has, at the same time, a large value of the two-nucleon relative momentum \mathbf{k}_{rel} and a low value of the c.m. momentum $\mathbf{K}_{\text{c.m.}}$, in agreement with the phenomenological assumption of Ref. [25]. The presence of SRCs in nuclei and their basic back-to-back nature have eventually been experimentally demonstrated [26–31], but a detailed theoretical and experimental information through the periodic Table of Elements of their isospin, angular and c.m. momentum dependencies remains to be obtained. To contribute to this challenge in the present paper the results of calculations of the following quantities, pertaining to nuclei ^3He , ^4He , ^{12}C , ^{16}O and ^{40}Ca , will be presented: (i) the two-nucleon momentum distribution $n_A^{N_1 N_2}$ of the proton-neutron (pn) and proton-proton (pp) pairs in correspondence of different values of the c.m. and the relative momenta of the pair and the angle Θ between them; (ii) the number of short-range correlated pp and pn pairs represented by the integral of the various types of momentum distributions in a finite momentum range; (iii) the ratio of the pn to pp correlated pairs *vs* the relative momentum k_{rel} . Particular attention is devoted to the comparison of the two-nucleon momentum distributions of complex nuclei with the deuteron momentum distribution, in order to clarify whether and to which extent the short-range dynamics of a free bound pn system will differ from the short-range dynamics of a pn pair embedded in the medium. Calculations have been performed with realistic nuclear wave functions [15, 32–34] obtained from the solution of the Schrödinger equation with realistic NN interactions, namely the AV18 [35] and AV8' [36] interactions. Various properties of the momentum distributions and various relations between them are illustrated, which further demonstrate the relevant property of the nuclear wave function in the correlation region, *i.e.* its factorized form. The quantity (the *nuclear contact*) measuring the number of deuteron-like pairs in nuclei is extracted from the general properties of the pn momentum distributions. The structure of the paper is as follows: in Section II the general definitions of the two-nucleon momentum distributions and their SRCd parts are given; the calculation of the momentum distributions and the universal, A-independent behavior of their SRCd parts, are presented in Section III; the general validity of the factorization property in the SRC region is proved in Section IV; the number of SRCd pn and pp pairs in various regions of k_{rel} and $K_{\text{c.m.}}$ are given in Section V; the comparison between the available experimental data with theoretical predictions is presented in Section VI; the Summary and Conclusions are illustrated in Section VII.

II. GENERAL DEFINITIONS

In this paper the number of protons and neutrons in nucleus A, will be denoted by Z and N, respectively, with

A = Z + N. The two-body momentum distributions of a pair of nucleons $N_1 N_2$, summed over spin (S) and isospin (T) states, is given by

$$n_A^{N_1 N_2}(\mathbf{k}_1, \mathbf{k}_2) = \frac{1}{(2\pi)^6} \int d\mathbf{r}_1 d\mathbf{r}_2 d\mathbf{r}'_1 d\mathbf{r}'_2 e^{i\mathbf{k}_1 \cdot (\mathbf{r}_1 - \mathbf{r}'_1)} e^{i\mathbf{k}_2 \cdot (\mathbf{r}_2 - \mathbf{r}'_2)} \rho_{N_1 N_2}^{(2)}(\mathbf{r}_1, \mathbf{r}_2; \mathbf{r}'_1, \mathbf{r}'_2), \quad (1)$$

where

$$\rho_{N_1 N_2}^{(2)}(\mathbf{r}_1, \mathbf{r}_2; \mathbf{r}'_1, \mathbf{r}'_2) = \int \psi_o^*(\mathbf{r}_1, \mathbf{r}_2, \mathbf{r}_3, \dots, \mathbf{r}_A) \psi_o(\mathbf{r}'_1, \mathbf{r}'_2, \mathbf{r}_3, \dots, \mathbf{r}_A) \delta\left(\sum_{i=1}^A \mathbf{r}_i\right) \prod_{i=3}^A d\mathbf{r}_i, \quad (2)$$

is the two-body non-diagonal density matrix of nucleus A. The normalization of the proton, neutron and total distributions, unless differently stated, is as follows¹

$$\begin{aligned} \int n_A^{N_1 N_2}(\mathbf{k}_1, \mathbf{k}_2) d\mathbf{k}_1 d\mathbf{k}_2 &= \int \rho_{N_1 N_2}^{(2)}(\mathbf{r}_1, \mathbf{r}_2) d\mathbf{r}_1 d\mathbf{r}_2 \\ &= \frac{Z(Z-1)}{2} \Big|_{N_1=N_2=p} \\ &= \frac{N(N-1)}{2} \Big|_{N_1=N_2=n} \\ &= ZN \Big|_{N_1=p, N_2=n} \end{aligned} \quad (3)$$

with

$$\begin{aligned} \sum_{N_1 N_2} \int n_A^{N_1 N_2}(\mathbf{k}_1, \mathbf{k}_2) d\mathbf{k}_1 d\mathbf{k}_2 \\ = \sum_{N_1 N_2} \int \rho_{N_1 N_2}^{(2)}(\mathbf{r}_1, \mathbf{r}_2) d\mathbf{r}_1 d\mathbf{r}_2 = \frac{A(A-1)}{2}. \end{aligned} \quad (4)$$

By introducing the relative and c.m. two-nucleon coordinates and momenta ($\mathbf{r} = \mathbf{r}_1 - \mathbf{r}_2$, $\mathbf{k}_{\text{rel}} = (\mathbf{k}_1 - \mathbf{k}_2)/2$; $\mathbf{R} = (\mathbf{r}_1 + \mathbf{r}_2)/2$, $\mathbf{K}_{\text{c.m.}} = \mathbf{k}_1 + \mathbf{k}_2$), the two-nucleon

momentum distribution can be rewritten as follows [10]:

$$\begin{aligned} n_A^{N_1 N_2}(\mathbf{k}_{\text{rel}}, \mathbf{K}_{\text{c.m.}}) &= n_A^{N_1 N_2}(k_{\text{rel}}, K_{\text{c.m.}}, \Theta) \\ &= \frac{1}{(2\pi)^6} \int d\mathbf{r} d\mathbf{R} d\mathbf{r}' d\mathbf{R}' e^{i\mathbf{K}_{\text{c.m.}} \cdot (\mathbf{R} - \mathbf{R}')} \\ &\quad e^{i\mathbf{k}_{\text{rel}} \cdot (\mathbf{r} - \mathbf{r}')} \rho_{N_1 N_2}^{(2)}(\mathbf{r}, \mathbf{R}; \mathbf{r}', \mathbf{R}'), \end{aligned} \quad (5)$$

where $|\mathbf{k}_{\text{rel}}| \equiv k_{\text{rel}}$, $|\mathbf{K}_{\text{c.m.}}| \equiv K_{\text{c.m.}}$ and Θ is the angle between \mathbf{k}_{rel} and $\mathbf{K}_{\text{c.m.}}$. Of particular interest is the quantity

$$\begin{aligned} n_A^{pn}(k_{\text{rel}}, K_{\text{c.m.}} = 0) \\ = \frac{1}{(2\pi)^3} \int d\mathbf{r} d\mathbf{r}' e^{i\mathbf{k}_{\text{rel}} \cdot (\mathbf{r} - \mathbf{r}')} \rho_{pn}^{(2)}(\mathbf{r}, \mathbf{r}'), \end{aligned} \quad (6)$$

describing the spin and isospin summed relative momentum distributions of BB pairs, $\rho_{pn}^{(2)}(\mathbf{r}, \mathbf{r}')$ being the c.m. integrated non-diagonal two-body density matrix. Relevant quantities are also the $K_{\text{c.m.}}$ - and k_{rel} -integrated momentum distributions, namely

$$n_A^{N_1 N_2}(k_{\text{rel}}) = \int n_A^{N_1 N_2}(\mathbf{k}_{\text{rel}}, \mathbf{K}_{\text{c.m.}}) d\mathbf{K}_{\text{c.m.}} \quad (7)$$

and

$$n_A^{N_1 N_2}(K_{\text{c.m.}}) = \int n_A^{N_1 N_2}(\mathbf{k}_{\text{rel}}, \mathbf{K}_{\text{c.m.}}) d\mathbf{k}_{\text{rel}}. \quad (8)$$

Eqs. (6), (7) and (8) have been calculated in Refs. [7, 8], [9], [10] and [11] for ${}^3\text{He}$ and ${}^4\text{He}$, using *ab initio* wave functions and in Ref. [11] for ${}^6\text{He}$, ${}^8\text{He}$, ${}^6\text{Li}$, ${}^7\text{Li}$, ${}^8\text{Li}$, ${}^9\text{Li}$, ${}^8\text{Be}$, ${}^9\text{Be}$, ${}^{10}\text{Be}$, ${}^{10}\text{B}$ and, preliminarily, ${}^{12}\text{C}$, within the VMC approach. In this paper we describe new results for various momentum distributions in ${}^3\text{He}$, ${}^4\text{He}$,

¹ Note that in Ref. [10] the two-nucleon momentum distributions were normalized to one in the case of ${}^4\text{He}$, whereas in case of ${}^3\text{He}$ it was normalized to the number of *pn* and *pp* pairs *i.e.* two and one, respectively

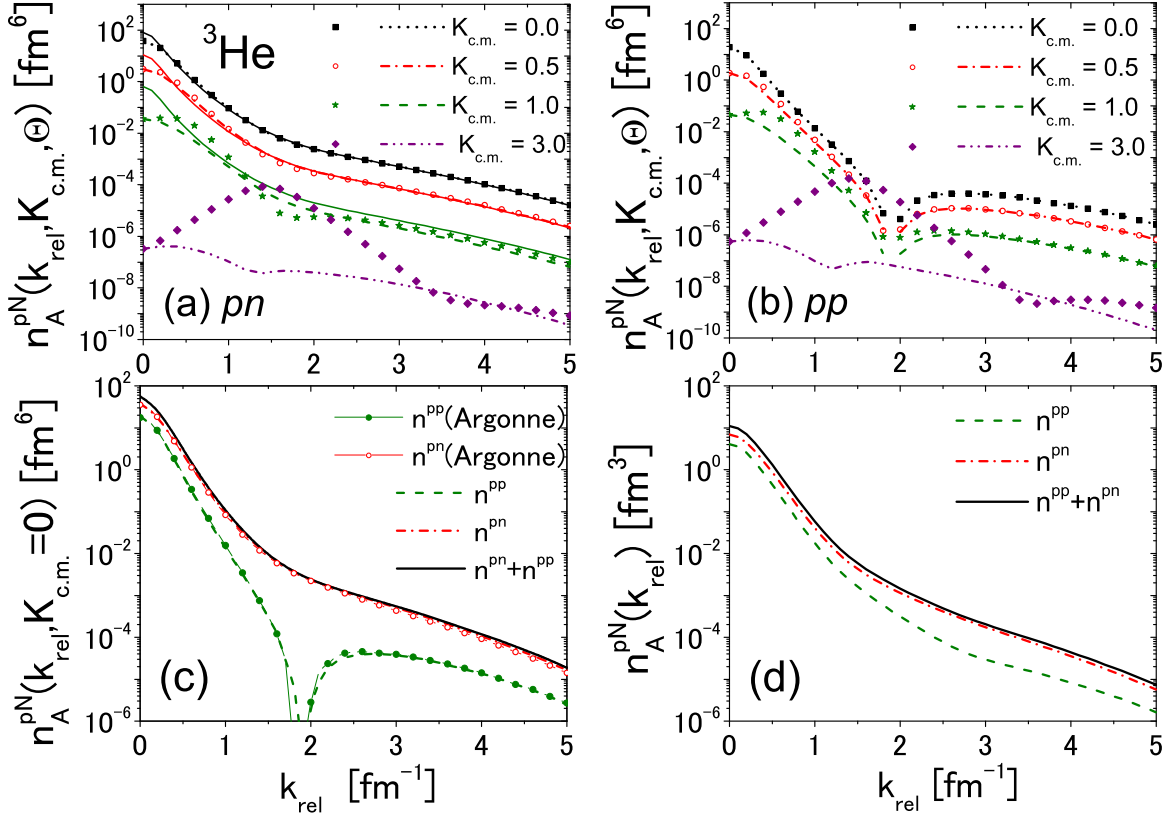


FIG. 1: (Color online): (a): the two-nucleon momentum distributions of pn pairs in ${}^3\text{He}$ vs. the relative momentum k_{rel} for fixed values of the c.m. momentum $K_{\text{c.m.}}$ (expressed in fm^{-1}) and two values of the angle Θ between \mathbf{k}_{rel} and $\mathbf{K}_{\text{c.m.}}$, namely $\Theta = 90^\circ$ (broken curves) and $\Theta = 0^\circ$ (symbols). In this Figure, and only in it, the continuous curves represent Eq. (10) with $C_3^{pn} = 2.0$. ${}^3\text{He}$ wave function from Ref. [32, 33] and AV18 interaction [35]. (b): the same as in Fig.1(a) but for pp pairs. (c): the pn and pp distributions corresponding to $K_{\text{c.m.}} = 0$ in (a) and (b) and their sum. (d): the relative two-body momentum distributions $n_A^{N_1 N_2}(k_{\text{rel}}) = \int n_A^{N_1 N_2}(\mathbf{k}_{\text{rel}}, \mathbf{K}_{\text{c.m.}}) d\mathbf{K}_{\text{c.m.}}$. In Fig. 1(c) the open and solid dots represent the results from Argonne [11]. In this and the following Figures, unless differently stated, the pn and pp distributions are normalized to ZN and $Z(Z-1)/2$, respectively.

${}^{12}\text{C}$, ${}^{16}\text{O}$ and ${}^{40}\text{Ca}$ obtained, in the case of few-nucleon systems ($A = 3, 4$), with *ab initio* wave functions, and, in the case of nuclei with $A > 4$, within a linked-cluster expansion up to the order of four-body cluster contributions [15]. Whenever possible the results of our calculations of the momentum distributions will be compared with the results of the VMC approach of Ref. [11]².

² In this paper we mainly discuss the spin-isospin summed momentum distributions of isoscalar nuclei whereas the spin-isospin dependent momentum distribution of non isoscalar nuclei will be the object of future investigations.

III. RESULTS OF CALCULATIONS AND THE UNIVERSAL PROPERTIES OF THE CORRELATED TWO-NUCLEON MOMENTUM DISTRIBUTIONS

A. The two-nucleon momentum distribution in ${}^3\text{He}$ and isoscalar nuclei

In Figs. 1-6 we show: (i) the pn and pp momentum distributions in ${}^3\text{He}$, ${}^4\text{He}$, ${}^{12}\text{C}$, ${}^{16}\text{O}$ and ${}^{40}\text{Ca}$ nuclei, in particular, the full two-nucleon momentum distribution $n_A^{N_1 N_2}(k_{\text{rel}}, K_{\text{c.m.}}, \Theta)$ (Eq. (5)), (ii) the back-to-back momentum distributions (Eq. (6)), (iii) the relative momentum distributions, Eq. (7) and (iv) the c.m. momentum

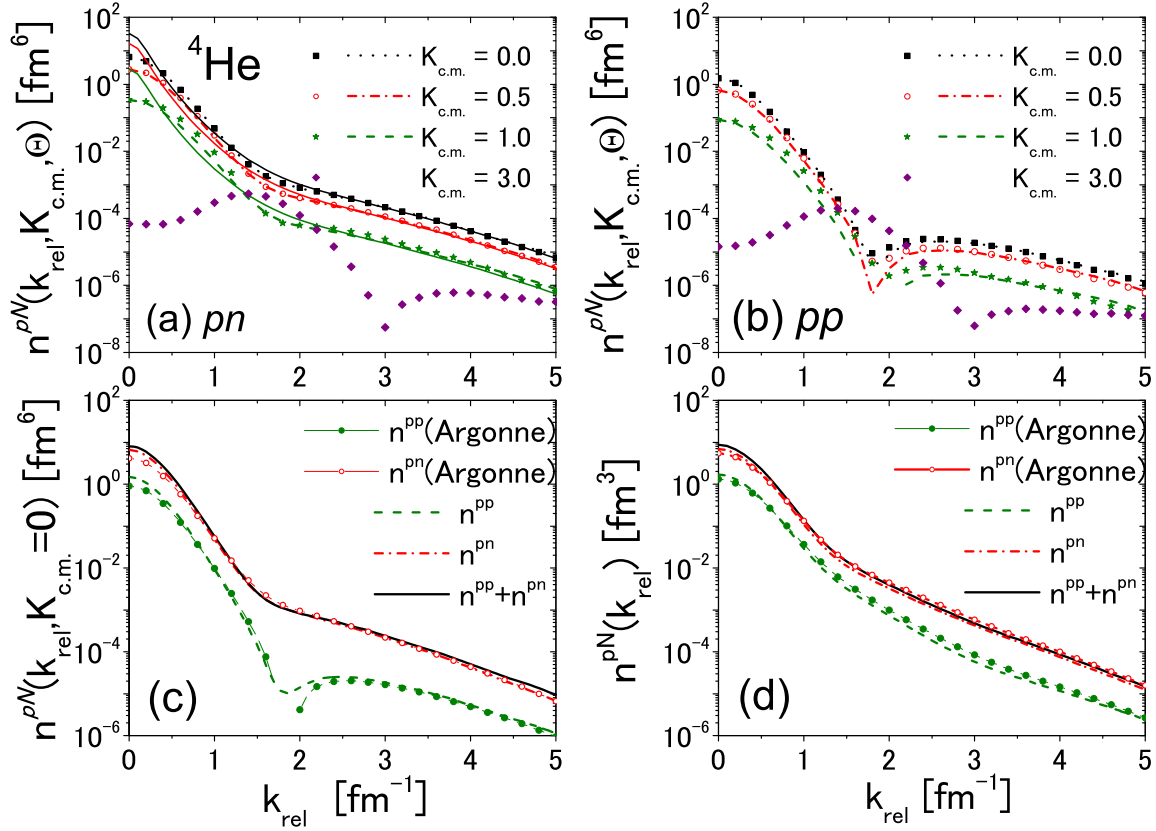


FIG. 2: (Color online) The same as in Fig. 1 but for ${}^4\text{He}$ with $C_4^{pn} = 4.0$ in Fig.2(a). ${}^4\text{He}$ wave function from Ref. [34] and AV8' interaction [36]. In Figs. 2(c) and 2(d) the open and solid dots denote the results from Argonne [11].

distribution, (Eq. (8)). The results presented in these Figures have been obtained using microscopic wave functions corresponding to the AV18 interaction [35] for ${}^2\text{H}$ and ${}^3\text{He}$ [32, 33] and the AV8' interaction [36] for ${}^4\text{He}$ [34] and complex nuclei [15]. In order to compare our results with the VMC results of Ref. [11], whose wave functions are calculated with 2N AV18+ 3N UX interaction, we present in Fig. 7 the one-nucleon momentum distributions of $A = 4$ and $A = 12$ obtained by the two approaches, even because both quantities will be used in what follows. Concerning our parameter-free results, let us first of all stress that they are in a general reasonable agreement with the results of the VMC calculation [11], although in some regions of momenta (e.g. at $2.5 \lesssim k_{rel} \lesssim 3.5 \text{ fm}^{-1}$) they can appreciably differ within a 10-20 %, particularly in the case of the pp relative momentum distribution of ${}^4\text{He}$ and ${}^{12}\text{C}$; the possible origin of such a disagreement, which does not appear to be given to the effects of the 3N force missing in our calculation [37], is under investigation. The obtained momentum distributions of both few-nucleon systems and complex nuclei exhibit several universal features that can be summarized as follows:

1. as firstly pointed out in Ref. [9] in the case of few-

nucleon systems, when $K_{c.m.} = 0$, the pn and pp momentum distributions do not appreciably differ at small values of k_{rel} , with their ratio being closer to the ratio of the number of pn to pp pairs, whereas in the region $1.0 \lesssim k_{rel} \lesssim 4.0 \text{ fm}^{-1}$ the dominant role of tensor correlations makes the pn distributions much larger than the pp distribution, with the node exhibited by the latter filled up by the D wave in the pn two-body density;

2. Figs. 1(a), (b) and 2(a), (b) show that the momentum distribution $n_A^{NN}(k_{rel}, K_{c.m.}, \Theta)$, plotted *vs.* k_{rel} , decreases, at small and high values of k_{rel} , with increasing values of $K_{c.m.}$, whereas at intermediate values of k_{rel} it increases with increasing values of $K_{c.m.}$; this effect is particularly relevant for the pp case where the dip occurring in the $K_{c.m.} = 0$ distribution is totally washed out by the large $K_{c.m.}$ components, resulting in a $K_{c.m.}$ -integrated distribution totally different from the one corresponding to $K_{c.m.} = 0$ (*cf.*); this effect seems to hold in the case of complex nuclei as well, as illustrated by the differences exhibited by Figures (b) and (c) for $A=12, 16$, and 40 .

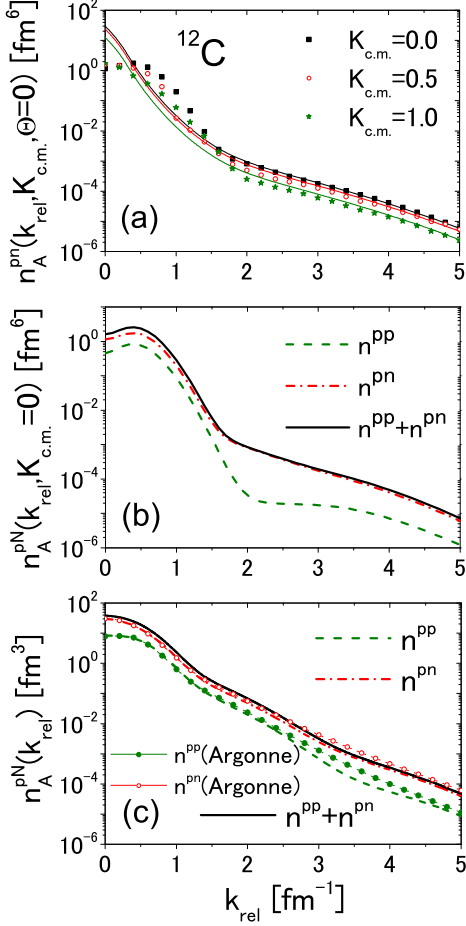


FIG. 3: (Color online): the same as in Fig. 1 but for ^{12}C with $C_{12}^{pn} = 20.0$ in Fig.3(a). ^{12}C wave function from Ref. [15] and AV8' interaction [36]. Note that in this Figure, as well as in Fig. 4 and 5 symbols in Figs. (a) correspond to $\Theta = 0$. In Fig. 3(c) the open and solid dots represent the results from Argonne [11].

- starting from a $K_{c.m.}$ -dependent value of the relative momentum k_{rel} , to be denoted $k_{rel}^-(K_{c.m.})$, the pn two-nucleon momentum distributions become to a large extent Θ independent, with the value of $k_{rel}^-(K_{c.m.})$ increasing with $K_{c.m.}$, according to the following relation

$$k_{rel}^-(K_{c.m.}) = a_1 + f(K_{c.m.}) \equiv k_{rel}^-; \quad (9)$$

that can be defined with $a_1 \simeq 1.5 \text{ fm}^{-1}$ (cf Figs. 1-5) and $f(K_{c.m.}) = K_{c.m.}$; Θ independence, firstly stressed in Ref. [17] and verified in a wide range of angles, implies that for $k_{rel} > k_{rel}^-$ the two-nucleon momentum distribution factorizes, *i.e.* $n_A^{N_1 N_2}(k_{rel}, K_{c.m.}, \Theta) \propto n_{rel}^{N_1 N_2}(k_{rel}) n_{c.m.}^{N_1 N_2}(K_{c.m.})$. In the region of factorization, defined by $k_{rel} \gtrsim k_{rel}^-$

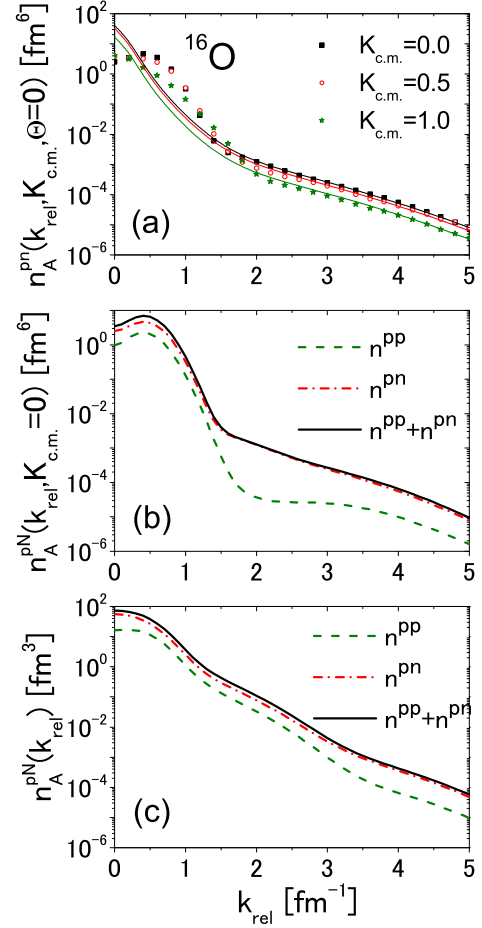


FIG. 4: (Color online) The same as in Fig. 1 but for ^{16}O with $C_{16}^{pn} = 24.0$ in Fig. 4(a). ^{16}O wave function from Ref. [15] and AV8' interaction [36].

and $K_{c.m.} \lesssim 1 \text{ fm}^{-1}$, the momentum distribution for pn pairs can be approximated as follows:

$$\begin{aligned} n_A^{pn(fact)}(k_{rel}, K_{c.m.}) &\simeq \frac{n_A^{pn}(k_{rel}, K_{c.m.} = 0)}{n_{c.m.}^{pn}(K_{c.m.} = 0)} n_{c.m.}^{pn}(K_{c.m.}) \\ &\simeq C_A^{pn} n_D(k_{rel}) n_{c.m.}^{pn}(K_{c.m.}). \end{aligned} \quad (10)$$

Here $n_D(k_{rel})$ is the deuteron momentum distribution, $n_{c.m.}^{pn}(K_{c.m.})$ the c.m. momentum distribution of the correlated pair in the region of factorization and C_A^{pn} an A-dependent constant, whose value and physical meaning will be discussed in the next Subsection. As for the pp momentum distribution, it appears that it also factorizes but starting at a value of the relative momentum higher than

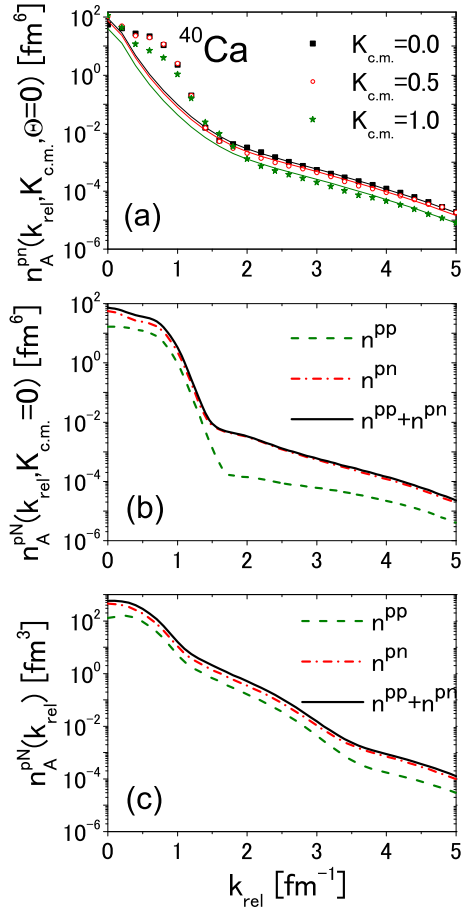


FIG. 5: (Color online) The same as in Fig. 1 but for ^{40}Ca with $C_{40}^{np} = 60.0$ in Fig. 5(a). ^{40}Ca wave function from Ref. [15] and AV8' interaction [36].

$k_{\text{rel}}(K_{\text{c.m.}})^{-}$; one has anyway

$$\begin{aligned} n_A^{pp(\text{fact})}(k_{\text{rel}}, K_{\text{c.m.}}) &\simeq \frac{n_A^{pp}(k_{\text{rel}}, K_{\text{c.m.}} = 0)}{n_{\text{c.m.}}^{pp}(K_{\text{c.m.}} = 0)} n_{\text{c.m.}}^{pp}(K_{\text{c.m.}}) \\ &\simeq C_A^{pp} n_{\text{rel}}^{pp}(k_{\text{rel}}) n_{\text{c.m.}}^{pp}(K_{\text{c.m.}}). \end{aligned} \quad (11)$$

where, unlike the pn case, the momentum distribution $n_{\text{rel}}^{pp}(k_{\text{rel}})$ is, at the moment, not defined in terms of a pp system. Eqs. (10) and (11) describe a property exhibited in Figs. 1 and 2 (and common to any value of A), namely that at high values of $k_{\text{rel}} > k_{\text{rel}}^-(K_{\text{c.m.}})$ the pN momentum distributions differ only by their magnitudes, which are governed by $n_{\text{c.m.}}^{pN}$;³

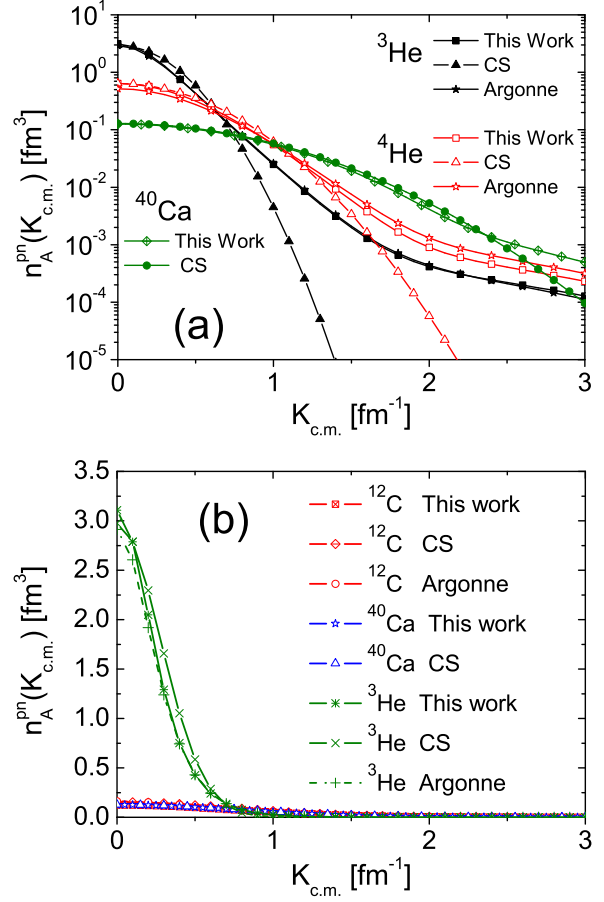


FIG. 6: (Color online)(a): The center-of-mass momentum distribution $n_A^{pn}(K_{\text{c.m.}}) = \int n_A^{pn}(\mathbf{k}_{\text{rel}}, \mathbf{K}_{\text{c.m.}}) d^3\mathbf{k}_{\text{rel}}$ (Eq. (8)) in ^3He , ^4He , ^{12}C and ^{40}Ca normalized to one, obtained in the present paper (*this work*), in Ref. [25] (*CS*) and in Ref. [11] (*Argonne*). Note that a Gaussian distribution related to the average value of the shell model kinetic energy [25] agrees very well with the many-body realistic distribution up to $K_{\text{c.m.}} \simeq 1 \text{ fm}^{-1}$ except in the case of ^3H for which a shell model description has no meaning. (b): the c.m. momentum distributions of ^3He , ^{12}C and ^{40}Ca on a linear scale.

- at high values of the relative and c.m. momenta, more than two particles can be locally correlated, producing a strong dependence upon the angle Θ and, correspondingly, the violation of factorization, as shown in Fig. 1 in the case of $K_{\text{c.m.}} = 3 \text{ fm}^{-1}$; moreover, it can be seen (*cf* Fig. 1(b) and 2(b)) that the behavior of n_A^{pp} in the region around $k_{\text{rel}} \simeq 2 \text{ fm}^{-1}$ is strongly affected by the high $K_{\text{c.m.}}$.

tum components, whereas $n_{\text{c.m.}}^{N_1 N_2}(K_{\text{c.m.}})$ has to describe only the low-momentum part ($K_{\text{c.m.}} \lesssim 1 - 1.5 \text{ fm}^{-1}$) of the c.m. motion

³ Note that $n_A^{N_1 N_2}(K_{\text{c.m.}})$ (Eq. (8)) includes all c.m. momen-

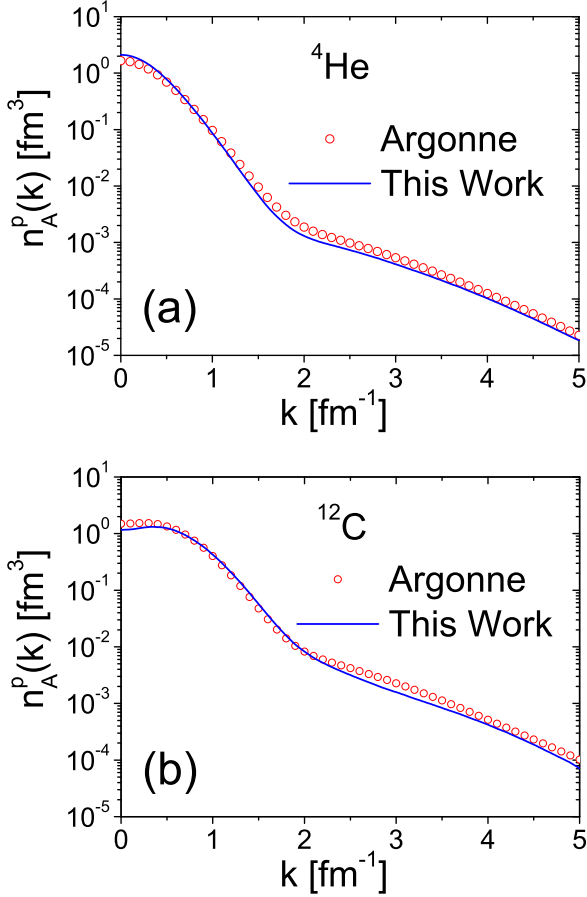


FIG. 7: (Color online) (Comparison of the one-nucleon momentum distributions of ^4He and ^{12}C calculated in Ref. [17] (full line) and in Ref. [11] (open dots), respectively. Normalization to the number of protons Z .

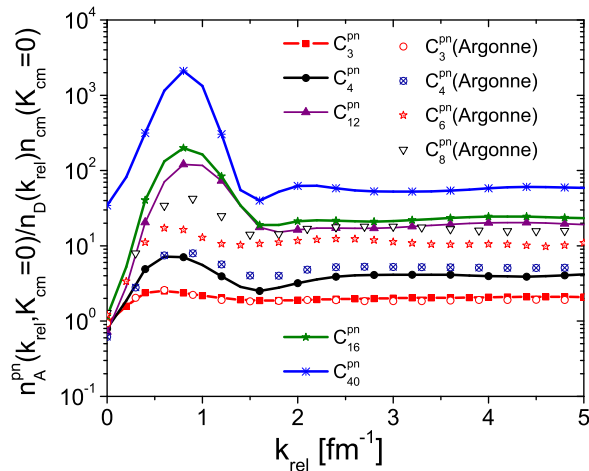


FIG. 8: (Color online) Determining the constant C_A^{pn} by a plot of Eq. (12) vs k_{rel} and fixed value of $K_{c.m.} = 0$. The constant value of Eq. (12) determines the value of C_A^{pn} . For ^3He , ^4He , ^6Li and ^8Be the results obtained with the Argonne momentum distributions [11] are also shown.

momentum components;

- in Ref. [25] the low momentum part ($K_{c.m.} \lesssim 1.0 \text{ fm}^{-1}$) of the $c.m.$ momentum distribution has been described by a gaussian function normalized to one, namely, $n_{c.m.}^A(K_{c.m.}) = (\alpha_A/\pi)^{3/2} \exp(-\alpha_A K_{c.m.}^2)$, with the values of α_A obtained from the average value of the shell model kinetic energy $\langle T \rangle_{SM}$, as follows $\alpha_A = \frac{3(A-1)}{4m_N(A-2)\langle T \rangle_{SM}}$. It can be seen from Fig. 6 that, apart from the case of ^3He , for which a shell-model description is meaningless, the Gaussian model of Ref. [25] nicely approximates the many-body result in the region of $K_{cm} \lesssim 1 \text{ fm}^{-1}$. The values of α_A for ^4He and ^{12}C obtained in Ref. [25] also agree with the experimental data [27, 28, 30], to be discussed in Section V.

B. The meaning and the numerical values of the quantity C_A^{pn}

In what follows we will discuss in detail the behavior of the pn momentum distributions in the correlation region, in particular the meaning and the numerical value of the constant C_A^{pn} appearing in Eq. (10). This is because we would like to compare the short-range behavior of a bound pn pair, *i.e.* the deuteron, with the behavior of a pn pair in the nuclear medium. The factorized form (Eq. (10)) describes 2N SRCd configurations when the relative momentum of the pair is much larger than the $c.m.$ momentum. Since for isoscalar nuclei $n_{c.m.}^{pn} \simeq n_{c.m.}^{pp}$, the A -dependence of $n_A^{pn(fact)}$ is given only by the A -dependence of both the constant C_A^{pn} and by the $c.m.$ momentum distribution $n_{c.m.}^{pn}$, with the former determining the amplitude of $n_A^{pn(fact)}(k_{rel}, K_{c.m.} = 0)$ and the latter its damping with increasing values of $K_{c.m.}$, as it clearly appears from Figs. 1-5, where can indeed be seen that the decrease of $n_A^{pn}(k_{rel}, K_{c.m.})$ at $k_{rel} > k_{rel}^-$ exactly follows the rate of decrease of $n_A^{pn}(K_{c.m.})$ shown in Fig. 6, whose low $K_{c.m.}$ distribution coincides with $n_{c.m.}^{pn}(K_{c.m.})$. Therefore it can be concluded that C_A^{pn} : (i) is independent of k_{rel} and $K_{c.m.}$, *i.e.* it is a quantity depending only upon the value of A , (ii) it is not a free and adjustable parameter, but a quantity resulting from *ab initio* many-body calculations of the momentum distributions, since, (iii) it is defined in terms of the magnitude of $n_A^{pn}(k_{rel}, K_{c.m.} = 0)$ at $k_{rel} \gtrsim k_{rel}^-$, the deuteron momentum distribution, and, eventually, by the $c.m.$ momentum distribution of the pair, *i.e.* by quantities resulting from many-body calculations and from the factorization property of the momentum distributions. To sum up, the value of C_A^{pn} is given by the following relation

$$\lim_{k_{rel} > k_{rel}^-} \frac{n_A^{pn}(k_{rel}, K_{c.m.} = 0)}{n_{c.m.}^{pn}(K_{c.m.} = 0)n_D(k_{rel})} = \text{Const} \equiv C_A^{pn} \quad (12)$$

^2H	^3He	^4He	^6Li	^8Be	^{12}C	^{16}O	^{40}Ca
1.0	2.0 ± 0.1	4.0 ± 0.1	—	—	20 ± 1.6	24 ± 1.8	60 ± 4.0
1.0	(2.0 ± 0.1)	(5.0 ± 0.1)	(11.1 ± 1.3)	(16.5 ± 1.5)	(—)	(—)	(—)

TABLE I: The values of the constant C_A^{pn} (Eq. (12)) extracted from Fig. 8, with error determined according to the following expression: $C_A^{pn} = \frac{(C_A^{pn})^{Max} + (C_A^{pn})^{Min}}{2} \pm \frac{(C_A^{pn})^{Max} - (C_A^{pn})^{Min}}{2}$, where $(C_A^{pn})^{Max}$ and $(C_A^{pn})^{Min}$ are determined in the region of $k_{rel} \geq 3.0 fm^{-1}$. The values in brackets have been obtained using the VMC wave function of Ref. [11]

The validity of Eq. (12) and the determination of the value of C_A^{pn} are illustrated in Fig. 8. It can be seen that at low values of the relative momentum ($k_{rel} \lesssim 1.5 fm^{-1}$) the ratio Eq. (12) exhibits a strong dependence upon k_{rel} , reflecting the A-dependent mean-field structure whereas, starting from $k_{rel} \simeq 2 - 2.5 fm^{-1}$, a constant behavior is observed for all values of A that have been considered; in particular, in the case of $A = 3$ and $A = 4$, for which accurate wave functions have been used, the consistency with a constant value is very good, whereas for complex nuclei, which are more sensitive to the many-body approximations, the error on the determination of the value of C_A^{pn} is higher. The obtained values of C_A^{pn} are listed in Table I, where the values obtained with the VMC results of Ref. [11] are also shown in brackets. The difference in the value of $C_{A=4}^{pn}$ between ours and the VMC approaches could be attributed to the different Hamiltonian (V8' NN interaction in our case and AV18 in VMC method) and to the different variational wave functions, whereas in the case of heavier nuclei possible effects from the omitted terms of the cluster expansion should also be considered. All of these possibilities are under investigation. Nonetheless the results of both approaches exhibit the same A-dependency, *i.e.* an increase of the value of C_A^{pn} with the value of A, which confirms the factorization property of the momentum distribution and that can be explained with the very physical meaning of C_A^{pn} . As a matter of fact Eq. (10) provides the physical meaning of the constant C_A^{pn} , namely in the factorization region one obtains

$$\begin{aligned}
& n_{pn}^{SRC,BB}(K_{c.m.} = 0) \\
&= \int_{k_{rel}^- = 1.5}^{\infty} d\mathbf{k}_{rel} \int_0^{\infty} n_A^{pn}(\mathbf{k}_{rel}, \mathbf{K}_{c.m.}) \delta(\mathbf{K}_{c.m.}) d\mathbf{K}_{c.m.} \\
&\simeq C_A^{pn} n_{c.m.}^{pn}(K_{c.m.} = 0) 4\pi \int_{k_{rel}^- = 1.5}^{\infty} n_D(k_{rel}) k_{rel}^2 dk_{rel}
\end{aligned} \tag{13}$$

which represents the momentum distribution of back-to-back (BB) nucleons integrated in the region of relative momentum $k_{rel} \geq 1.5 fm^{-1}$. Thus C_A^{pn} represent a measure of the number of SRCd pn pairs with c.m. momentum distribution $n_{c.m.}^{pn}(K_{c.m.} = 0)$, *i.e.* the number of

deuteron-like pairs. At the same time the equation

$$\begin{aligned}
N_{pn}^{SRC} &= \int_0^{K_{c.m.}^{max}} d\mathbf{K}_{c.m.} \int_{k_{rel}(K_{c.m.})}^{\infty} n_A^{pn}(\mathbf{k}_{rel}, \mathbf{K}_{c.m.}) d\mathbf{k}_{rel} \\
&\simeq C_A^{pn} (4\pi)^2 \int_0^{K_{c.m.}^{max}} n_{c.m.}^{pn}(K_{c.m.}) K_{c.m.}^2 dK_{c.m.} \\
&\int_{k_{rel}^-(K_{c.m.})}^{\infty} n_D(k_{rel}) k_{rel}^2 dk_{rel},
\end{aligned} \tag{14}$$

represents the the number of SRCd pn pairs in the entire two-nucleon SRC region, characterized by $K_{c.m.}^{max} \lesssim 1 \sim 1.5 fm^{-1}$ and $k_{rel}^- \gtrsim 1.5 fm^{-1}$ ⁴.

IV. THE FACTORIZATION PROPERTY OF THE NUCLEAR WAVE FUNCTION AND THE HIGH MOMENTUM BEHAVIOR OF THE MOMENTUM DISTRIBUTIONS

A. SRCs as a result of wave function factorization

It has been demonstrated that the the momentum distributions of nuclei in the region of SRCs are governed by the *factorization property* of the nuclear wave function at short inter-nucleon distances, described by the following relation

$$\begin{aligned}
& \lim_{r_{ij} \rightarrow 0} \Psi_0(\{\mathbf{r}\}_A) \\
& \simeq \hat{A} \left\{ \chi_o(\mathbf{R}_{ij}) \sum_{n, f_{A-2}} a_{o,n, f_{A-2}} \left[\Phi_n(\mathbf{x}_{ij}, \mathbf{r}_{ij}) \right. \right. \\
& \quad \left. \left. \oplus \Psi_{f_{A-2}}(\{\mathbf{x}\}_{A-2}, \{\mathbf{r}\}_{A-2}) \right] \right\},
\end{aligned} \tag{15}$$

where: i) $\{\mathbf{r}\}_A$ and $\{\mathbf{r}\}_{A-2}$ denote the set of radial coordinates of nuclei A and A - 2, respectively; (ii) \mathbf{r}_{ij} and \mathbf{R}_{ij} are the relative and c.m. coordinate of the nucleon pair ij , described by the relative wave function Φ_n and the c.m. wave function χ_o in 0s state; iii) $\{\mathbf{x}\}_{A-2}$ and \mathbf{x}_{ij} denote the set of spin-isospin coordinates of the

⁴ Following the original suggestion of Ref. [18] we also adopt here the region $k_{rel}^- \gtrsim 1.5 fm^{-1}$ as the *SRC region*, although, more correctly, as it appears from the results of many-body calculations, the *SRC region* starts from $k_{rel}^- \gtrsim 2 fm^{-1}$.

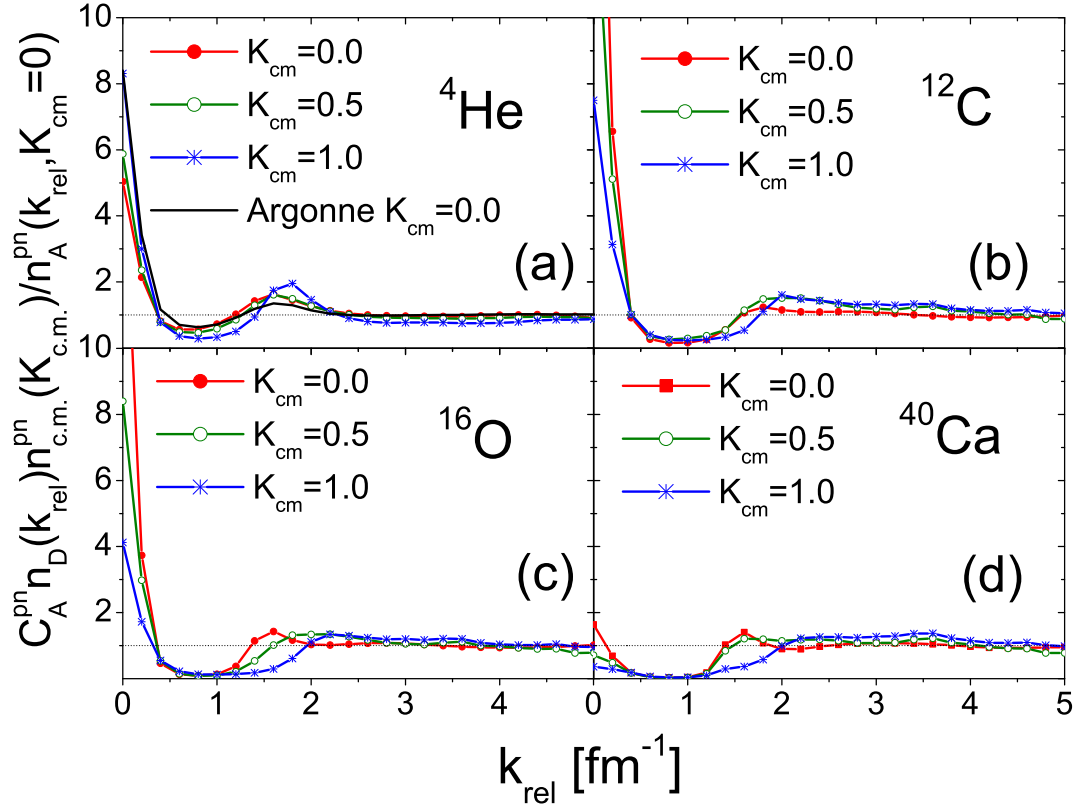


FIG. 9: (Color online) The ratio (Eq. (16)) between the factorized distributions (Eq. (10)) and the exact ones ($\Theta = 0^\circ$) for ^4He , ^{12}C , ^{16}O and ^{40}Ca in correspondence of $K_{c.m.} = 0, 0.5, 1 \text{ fm}^{-1}$. For ^4He the results obtained with the Argonne momentum distributions [11] are shown by the full line.

nucleus ($A - 2$) and the pair (ij). Eq. (15) has been introduced in [25] demonstrating that the SRCd nuclear two-nucleon momentum distribution factorizes into the

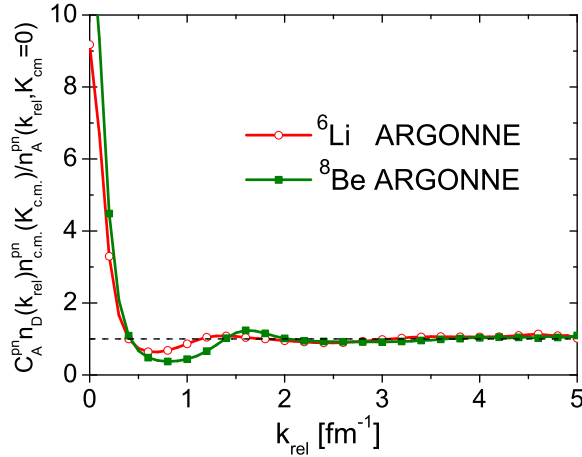


FIG. 10: (Color online) The ratio (Eq. (16)) between the factorized distributions, Eq. (10), and the exact ones for ^6Li and ^8Be , corresponding to $K_{c.m.} = 0$, obtained with the Argonne VMC wave functions [11].

vector-coupled product of the relative and c.m. momentum distribution of a NN pair. In particular, in Ref. [24] the factorization property of the nuclear wave function has been shown to hold in the case of *ab initio* wave functions of few-nucleon systems, showing that the momentum-space wave function of ^3He and ^4He factorize in the region of *high* ($k_{rel} \gtrsim 2 \text{ fm}^{-1}$) relative momenta coupled to *low* c.m. momenta, ($K_{c.m.} \lesssim 1.0 \text{ fm}^{-1}$), whereas at higher values of $K_{c.m.}$ factorization still occurs but starting at increasing values of k_{rel} ; such a behavior indeed appears in Figs. 1(a)-5(a), both in the case of few-nucleon systems and complex nuclei. Finally, in Ref [23], the factorization property of the wave function and momentum distribution have also been shown to occur in case of nuclear matter treated within the Brueckner-Bethe-Goldstone approach. In order to provide new evidence about the validity of the factorization property, we show in Figs. 9 and 10 the ratio of the factorized momentum distribution of a pn pair, Eq. (10) to the exact momentum distribution $n_A^{pn}(k_{rel}, K_{cm}, \Theta)$, *i.e.* the quantity

$$R_{fact/exact}^{pn} = \frac{C_A^{pn} n_D(k_{rel}) n_{c.m.}^{pn}(K_{c.m.})}{n_A^{pn}(k_{rel}, K_{cm}, \Theta)} \quad (16)$$

plotted on a linear scale. It can be seen that, independently of the nuclear mass and the values of $K_{c.m.}$, the ratio exhibits, at $k_{rel} \gtrsim 2 fm^{-1}$, a constant value equal to one. The scaling to one is perfect for $A = 4, 6, 8$ nuclei for which *ab initio* VMC momentum distributions have been used, whereas it presents small oscillations for complex nuclei, a behavior that should be attributed to the approximations which have been used to solve the many-body problem.

B. Wave function factorization and the relation between the relative momentum distribution of pn pairs in nuclei and the deuteron momentum distributions

In Fig.11 the two-nucleon momentum distributions of pn pairs in nuclei is compared with the deuteron momentum distribution. As already pointed out, the in-medium pn momentum distribution is a relevant quantity for the study of in-medium dynamics since it represents a unique opportunity to compare the properties of a free bound pn system with the properties of a pn system embedded in the medium. The ratio

$$R_{pn/D}(k_{rel}, K_{c.m.} = 0) = \frac{n_A^{pn}(k_{rel}, K_{c.m.} = 0)}{C_A^{pn} n_{c.m.}^{pn}(K_{c.m.} = 0)} \quad (17)$$

is presented in Fig.11(a), whereas the quantity

$$R_{pn/D}(k_{rel}) = \frac{n_A^{pn}(k_{rel})}{C_A^{pn}} \quad (18)$$

is shown in Figs.11(b), (c) and (d). The scaling of the Eq. (17) to the deuteron momentum distributions, starting from $k_{rel} \simeq 2 fm^{-1}$ is clearly exhibited and it can also be seen that scaling of $n_A^{pn}(k_{rel})$ also takes place (*cf* Eq (18)), but only at very large values of $k_{rel} \gtrsim 4 fm^{-1}$. These results are both obtained with our momentum distributions and with the VMC ones. By comparing Figs. 11(a) and (b) it can be concluded that the pn momentum distribution in nuclei is governed, at high value of the relative momentum, only by the deuteron-like momentum components, *i.e.* by the two-nucleon momentum distributions with $K_{c.m.} = 0$.

C. Wave function factorization and the relation between the one-nucleon and the two-nucleon momentum distributions. The one-nucleon momentum distribution vs the deuteron momentum distribution

The results presented in Fig. 9 and Fig. 10 represents unquestionable evidence of the validity of the factorization property, which leads to the convolution model (CONV) of the one-nucleon spectral function and momentum distributions describing both quantities in terms of a convolution integral of the relative and c.m. momentum distributions of a correlated pair [25]. Within

the CONV the exact relation between the one- and two-nucleon momentum distributions, namely (*e.g.* for protons)

$$n_A^p(\mathbf{k}_1) = \frac{1}{A-1} \left(\int n_A^{pn}(\mathbf{k}_1, \mathbf{k}_2) d\mathbf{k}_2 + 2 \int n_A^{pp}(\mathbf{k}_1, \mathbf{k}_2) d\mathbf{k}_2 \right) \quad (19)$$

is represented in the correlation region at high momenta by the following convolution integrals ($\mathbf{k}_1 + \mathbf{k}_2 + \mathbf{k}_3 = 0$, $\mathbf{k}_3 = \mathbf{K}_{A-2} = -\mathbf{K}_{c.m.} = -(\mathbf{k}_1 + \mathbf{k}_2)$)

$$n_A^p(\mathbf{k}_1) = \int n_{rel}^{pn}(|\mathbf{k}_1 - \frac{\mathbf{K}_{c.m.}}{2}|) n_{c.m.}^{pn}(\mathbf{K}_{c.m.}) d\mathbf{K}_{c.m.} + 2 \int n_{rel}^{pp}(|\mathbf{k}_1 - \frac{\mathbf{K}_{c.m.}}{2}|) n_{c.m.}^{pp}(\mathbf{K}_{c.m.}) d\mathbf{K}_{c.m.} \quad (20)$$

Eq. (20) establishes a relation between the one-nucleon momentum distribution $n_A^p(\mathbf{k}_1)$ and the relative and c.m. momentum distributions of the $N_1 N_2$ pair ⁵. At large values of \mathbf{k}_1 , such that $\mathbf{k}_1 \gg \mathbf{K}_{c.m.}/2$, the convolution formula could in principle be approximated by

$$n_A^p(k_1) \simeq n_{rel}^{pn}(k_{rel} = k_1) + 2n_{rel}^{pp}(k_{rel} = k_1) \quad (21)$$

which represents the contribution of back-to-back nucleons to the one-nucleon momentum distribution; Eq. (21) can also be expressed in the following equivalent form

$$n_A^p(k_1) = \frac{n_A^{pn}(k_{rel} = k_1, K_{c.m.} = 0)}{n_{c.m.}^{pn}(K_{c.m.} = 0)} + 2 \frac{n_A^{pp}(k_{rel} = k_1, K_{c.m.} = 0)}{n_{c.m.}^{pp}(K_{c.m.} = 0)} \quad (22)$$

as well as in the form

$$n_A^p(k_1) \simeq C_A^{pn} n_D(k_{rel} = k_1) + 2 \frac{n_A^{pp}(k_{rel} = k_1, K_{c.m.} = 0)}{n_{c.m.}^{pp}(K_{c.m.})}, \quad (23)$$

which establishes a clear-cut relation between the one-nucleon momentum distribution and the momentum distribution of the deuteron in case of pairs of nucleons with back-to-back ($K_{c.m.} = 0$) momenta ⁶. Starting from a factorized wave function, a relation similar to Eq. (21) has been obtained in Ref. [39], where however, instead of the relative momentum distribution $n_{rel}^{N_1 N_2}(k_{rel}) = n_A^{N_1 N_2}(k_{rel} = k_1, K_{cm} = 0)/n_{c.m.}^{N_1 N_2}(K_{c.m.} = 0)$, the K_{cm} -integrated relative momentum distributions (Eq.(7)) has been used. We will

⁵ In actual calculations of Ref. [25] the exact Eq. (20) has been approximated by using an effective two-nucleon momentum distribution.

⁶ Note that in the following, we use $n_{c.m.}^{pp}(K_{c.m.}) = n_{c.m.}^{pn}(K_{c.m.})$.

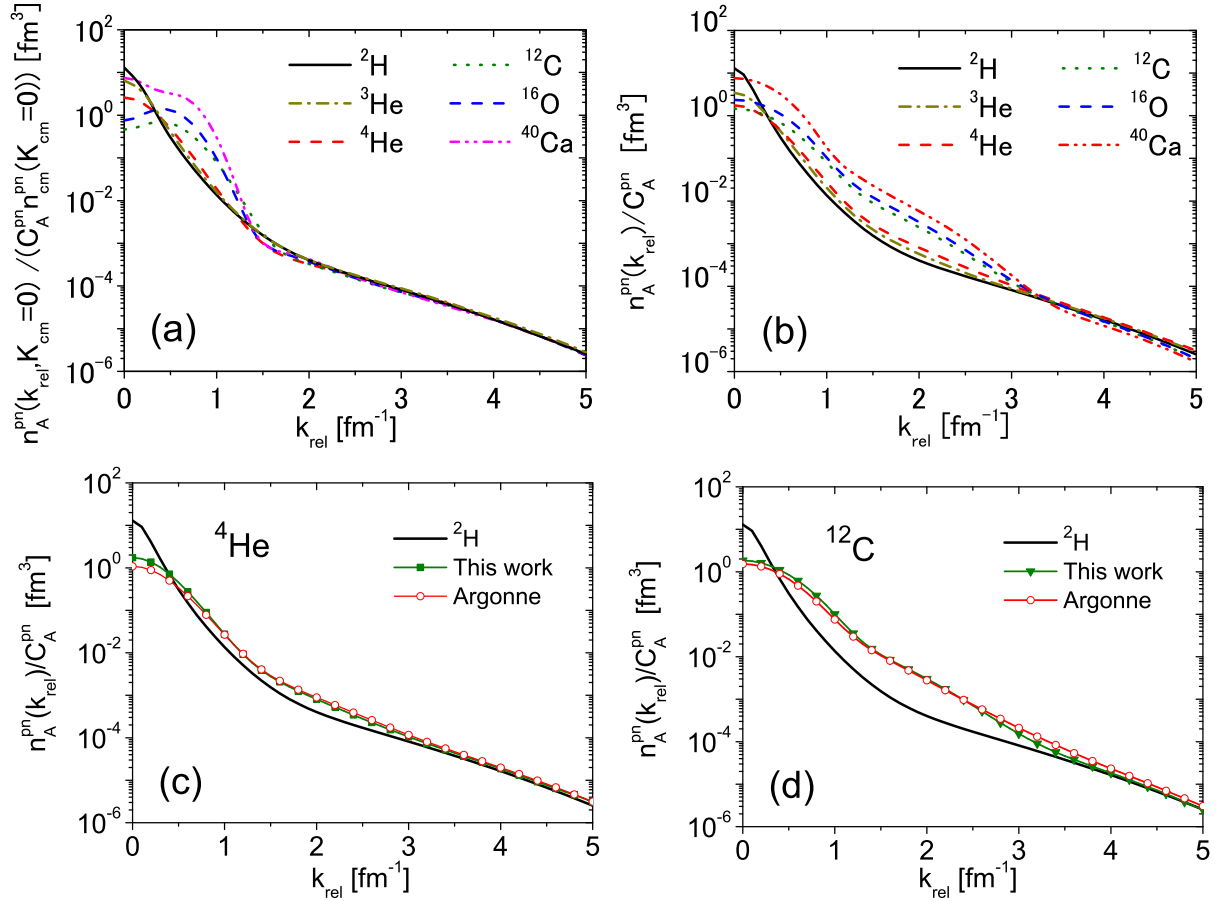


FIG. 11: (Color online) (UPPER PANEL): Comparison of the deuteron momentum distributions with the two-nucleon momentum distributions of various nuclei obtained in the present paper. Fig.(a) demonstrates the validity of the relation $n_A^{pn}(k_{rel}, K_{c.m.})/C_A^{pn} n_A^{pn}(K_{c.m.} = 0) \simeq n_D(k_{rel})$, when $K_{c.m.} = 0$ and $k_{rel} \gtrsim 2 \text{ fm}^{-1}$, whereas Fig.(b) demonstrates that when the $K_{c.m.}$ -integrated two-nucleon momentum distributions are considered the relation $n_A^{pn}(k_{rel})/C_A^{pn} \simeq n_D(k_{rel})$ is also valid but only at $k_{rel} \gtrsim 3.5 \sim 4 \text{ fm}^{-1}$. (LOWER PANEL): The quantity $n_A^{pn}(k_{rel})/C_A^{pn}$ for ^4He (c) and ^{12}C corresponding to the momentum distributions obtained in the present paper and in Ref. [11]. In both panels the values of C_A^{pn} are the ones given in Table I. These results unambiguously prove both $n_A^{pn}(k_{rel}, K_{c.m.} = 0)$ and $n_A^{pn}(k_{rel})$ do factorize to the deuteron momentum distribution but starting at appreciably different values of k_{rel} in the two cases. These results also show that $n_A^{pn}(k_{rel})$ at $k_{rel} \gtrsim 3.5 \sim 4 \text{ fm}^{-1}$ is mainly governed by back-to-back pn pairs.

show that, as expected from Fig. 11(a) and (b), the relation between the one- and two-body momentum distribution will be numerically different. Let us first of all analyze the validity of the convolution model. In Fig. 12 a detailed analysis of the model is presented for the ^4He nucleus. The following features *in the region of factorization dominated by SRCs* ($k \gtrsim 2 \text{ fm}^{-1}$), are worth being stressed: (i) the exact momentum distribution $n_A^p(k)$ is correctly approximated by the convolution formula (Eq. (20)) and, particularly, by its asymptotic behavior (Eq. (22)) including its deuteron-like character for the pn distribution *i.e.* for back-to-back SRCd nucleon pairs; (ii) the exact calculation, the calculation with the convolution formula, using there either $C_A^{pn} n_D(k_{rel})$ or $n_A^{pn}(k_{rel}, K_{c.m.} = 0)/n_{c.m.}^{pn}(K_{c.m.} = 0)$

for the relative motion, yield very similar results starting from $k_{rel} \gtrsim 2 \text{ fm}^{-1}$, whereas Eq. (22) with the $\mathbf{K}_{c.m.}$ -integrated relative momentum distribution reproduce $n_A^p(k)$ only when $k_{rel} \gtrsim 3.5 \sim 4 \text{ fm}^{-1}$. In order to further demonstrate the relationships of the one- and two-nucleon momentum distributions we show in Fig. 13 the ratios

$$R_{N_1 N_2 / N_1}^{BB}(k_1) = \frac{1}{n_A^p(k)} \left[\frac{n_A^{pn}(k_{rel}, K_{c.m.} = 0)}{n_{c.m.}^{pn}(K_{c.m.} = 0)} + 2 \frac{n_A^{pp}(k_{rel}, K_{c.m.} = 0)}{n_{c.m.}^{pp}(K_{c.m.} = 0)} \right] \quad (24)$$

and

$$R_{N_1 N_2 / N_1}^{int}(k_1) = \frac{n_A^{pn}(k_{rel}) + 2n_A^{pp}(k_{rel})}{n_A^p(k_1)}, \quad (25)$$

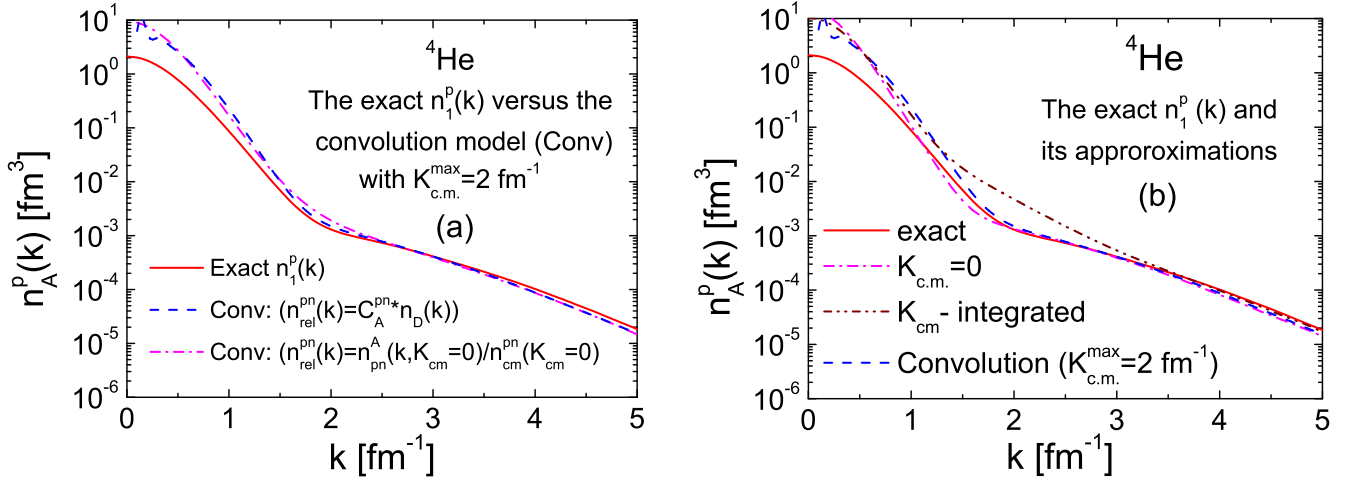


FIG. 12: (Color online) (a) The exact proton momentum distribution $n_A^p(k)$ ($k_1 \equiv k$) compared with the convolution model, Eq.(20) (Conv), calculated with two different expressions for $n_{\text{rel}}^{\text{pn}}$. (b) The exact $n_A^p(k)$ compared with: (i) the asymptotic approximation of convolution model (Eq. (21) and Eq. (22)) ($K_{\text{c.m.}} = 0$); (ii) Eq. (21) with $n_{\text{rel}}^{N_1 N_2}(k_1 = k_{\text{rel}})$ replaced by the $K_{\text{c.m.}}$ -integrated relative momentum distributions $n_A^{N_1 N_2}(k_{\text{rel}}) = \int n_A^{N_1 N_2}(\mathbf{k}_{\text{rel}}, \mathbf{K}_{\text{c.m.}}) d\mathbf{K}_{\text{c.m.}}$; (iii) the convolution model (Eq.(24)) as in (a).

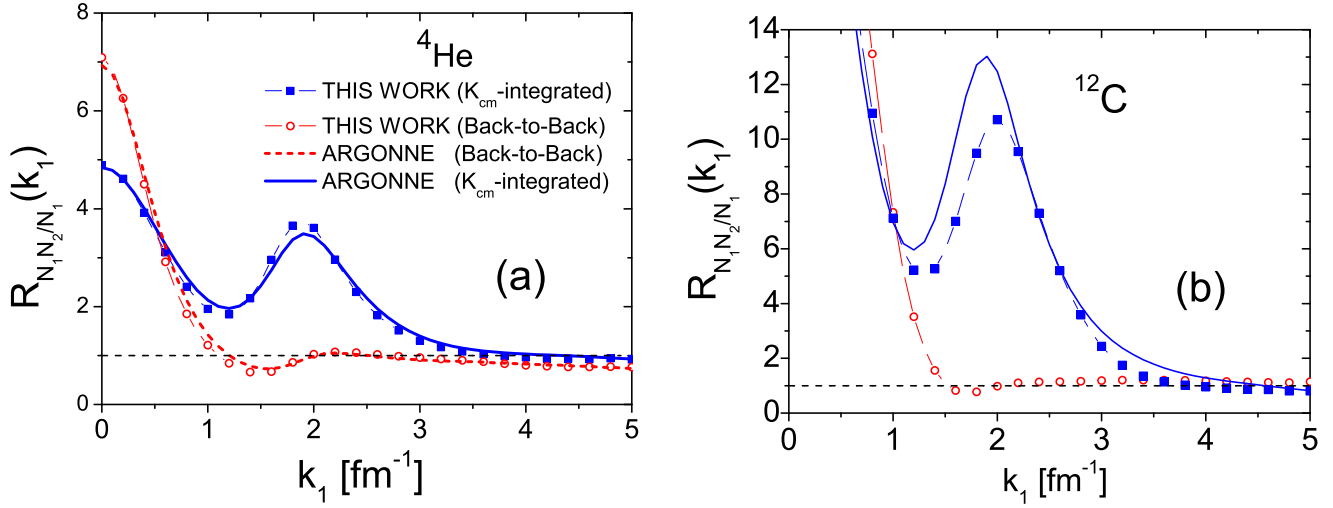


FIG. 13: (Color online) The ratio of the full two-nucleon momentum distribution $n_{pn} + 2n_{pp}$ to the one-nucleon momentum distribution n_A^p for ^4He (a) and ^{12}C (b) calculated using in the numerator the relative two-nucleon distributions $n_A^{\text{pn}}(k_{\text{rel}} = k_1, K_{\text{c.m.}} = 0) / n_{\text{c.m.}}(K_{\text{c.m.}} = 0)$ (Eq. (24), open dots), and (ii) the $\mathbf{K}_{\text{c.m.}}$ -integrated two-nucleon momentum distributions $n_A^{\text{pn}}(k_{\text{rel}})$ (Eq.(25), full squares); in both cases the numerator is the one-nucleon momentum distribution. The solid line denotes the results obtained with the Argonne VMC wave function [11].

where in both quantities n_A^p is the exact proton momentum distribution and the numerators differ in that in Eq. (24) back-to-back nucleon distributions are considered, unlike the case of Eq.(25) where the $\mathbf{K}_{\text{c.m.}}$ - integrated relative momentum distributions are adopted. The re-

gions of validity of the two cases, both corresponding to $k_1 \simeq k_{\text{rel}}$, *i.e.* $K_{\text{c.m.}} \simeq 0$ are determined by a constant value of the ratios. As expected from the results presented in Figs. 11 and 12, Eq. (24) is unity in a wider range of momenta. The results presented in Fig. 13 pro-

vide further evidence of the validity of both the factorization property and the convolution model, and tells us that when the ratios equals one, the one-nucleon momentum distribution is dominated by back-to-back configurations with $\mathbf{k}_1 = -\mathbf{k}_2 = \mathbf{k}_{rel}$, $\mathbf{K}_{c.m.} = 0$. Concerning the relationship of the one-nucleon momentum distributions and the momentum distributions of the deuteron, as already illustrated, this is given by Eq. (23). However, by plotting the ratio of the one-nucleon momentum distribution to the momentum distributions of the deuteron $R_{A/D}(k_1) = \frac{n_A^p(k_1)}{n_D(k_1)}$ the relationships between the two quantities can be exhibited in more detail, as quantitatively illustrated in Ref.[17]. There it has been shown that $N_{A/D}(k_1)$ never becomes constant, which means that $n_1^A(k_1)$ is not linearly proportional to $n_D(k_1)$; this is mostly due to the contribution of the pp distribution, which increases with increasing momentum k_1 , and to the c.m. motion of a pn pair in the nucleus and only if pp contributions are disregarded and only back-to-back pn pairs are considered, one indeed obtains that in the region $k_1 \gtrsim 2 fm^{-1}$, $n_A^p(k_1) \simeq C_A^{pn} n_D(k_1)$. The relation between the nucleon momentum distribution of nucleus A and the deuteron momentum distribution, has been and is still being used in the treatment of SRCs. Still now the proportionality of the nuclear momentum distribution to the momentum distribution of the deuteron is sometimes assumed, which is equivalent to the statement that the high momentum content of the nucleus is fully determined by the two-nucleon state (ST) = (10). In the past realistic calculations of the nuclear momentum distributions at high momenta could not be performed with sufficient accuracy and the similarity of the deuteron and the nuclear momentum distribution has been simply assumed, e.g. in the early VMC calculations [42] or in the development of workable models of the spectral function for complex nuclei [25]. Recent advanced calculations of the one- and two-body momentum distributions [3, 10, 11, 16, 17], including the results of the present paper, show that also states different from the deuteron one, namely the states (01) and (11), do contribute to the high momentum part of the momentum distributions, demonstrating, in the case of the state (11), that a considerable number of two-nucleon states with odd value of the relative orbital momentum is present in the realistic ground-state wave function of nuclei.

D. Wave function factorization and the nuclear contacts

The concept of *contact*, introduced by Tan in Ref. [38], to describe the short-range behavior of two unlike electrons in a two-component Fermi gas, has been recently discussed within the context of SRCs in nuclei (see e.g. Refs. [39, 40]). Although a detailed discussion of this topic is outside the aim of the present paper and will be discussed elsewhere, it is nevertheless useful to stress here that the *contacts*: (i) are quantities that measure

the probability to find two particles at short relative distances ([38, 39]) and, (ii) they are obtained, both in atomic and nuclear systems, by postulating a factorized wave functions of the form of Eq. (15) [39]. For these reasons, the quantity C_A^{pn} we have obtained, measuring the probability to have SRCd back-to-back pn pairs, represent nuclear pn contacts ⁷.

V. ON THE NUMBER OF HIGH-MOMENTUM SHORT-RANGE CORRELATED NUCLEON-NUCLEON PAIRS IN NUCLEI

Having at disposal the two-nucleon momentum distributions, the absolute values of the number of SRCd pairs, *i.e.* the integral of the two-nucleon momentum distributions in a given relative and c.m. momentum region, can be calculated and, as in the case of the deuteron, a proper definition of the probability of SRCs in a nucleus can be given. However in a complex nucleus the two-nucleon momentum distributions depend upon three variables so that, as pointed out in Ref. [17], there is a certain degree of ambiguity in providing a clear-cut definition of the probability of SRCs in terms of an integral of the two-nucleon momentum distributions. In the case of the deuteron, which is described only in terms of a back-to-back (BB) configuration ($\mathbf{k}_1 = -\mathbf{k}_2 = \mathbf{k}$, $\mathbf{k}_{rel} \equiv \mathbf{k}$, $\mathbf{K}_{c.m.} = 0$), a commonly adopted definition of the probability of SRCs is given by the integral of the momentum distribution $n_D(k)$ ($k_{rel} \equiv k$) in the interval $1.5 \leq k \leq \infty fm^{-1}$, which is the region dominated by the high momentum components generated by the repulsive core and by the deuteron D-wave produced by the tensor force. Therefore in the deuteron the total number of pn pairs is $N_D = 1$, and the number of back-to-back (BB) SRCd pn pairs is

$$N_D^{BB} = 4\pi \int_{k=1.5}^{\infty} n_D(k) k^2 dk \equiv N_{pn}^{BB} \simeq 0.036, (26)$$

i.e. only 4% of the pn pair is SRCd (such a percentage corresponds to the AV18 interaction). The extent to which such a probability will differ in a complex nucleus is a relevant issue, for it can provide information on in-medium effects on short-range pn dynamics. For this reason, a similar definition, *i.e.* the integral of the relative momentum distribution in the range $k_{rel} \gtrsim 1.5 fm^{-1}$, might also be introduced in the case of a complex nucleus, keeping however in mind that in a nucleus all possible values of $K_{c.m.}$ and Θ , as well as all four spin-isospin

⁷ It should be stressed that in case of nuclei four contacts, depending upon the spin-isospin state of the pair, can be defined; moreover, the contacts may be defined to depend upon the center-of-mass of the correlated pair, namely for a fixed value of the c.m. momentum, for back-to-back nucleons, as well as for the $\mathbf{K}_{c.m.}$ -integrated momentum distributions.

	^2H			^3He			^4He		
	$N_{N_1 N_2}^{BB}$	$N_D^{SRC,BB}$	$\mathcal{P}_D^{SRC,BB}$	$N_{N_1 N_2}^{BB}$	$N_{N_1 N_2}^{SRC,BB}$	$\mathcal{P}_{N_1 N_2}^{SRC,BB}$	$N_{N_1 N_2}^{BB}$	$N_{N_1 N_2}^{SRC,BB}$	$\mathcal{P}_{N_1 N_2}^{SRC,BB}$
pn	1	0.036	3.6	6.22	0.22	3.5	2.54	0.08	3.1
	(1)	(0.036)	(3.6)	(5.82)	(0.20)	(3.4)	(2.05)	(0.09)	(4.3)
pp	-	-	-	2.05	0.01	0.5	0.55	0.005	0.9
	-	-	-	(2.10)	(0.01)	(0.5)	(0.42)	(0.004)	(1.0)

	^{12}C			^{16}O			^{40}Ca		
	$N_{N_1 N_2}^{BB}$	$N_{N_1 N_2}^{SRC,BB}$	$\mathcal{P}_{N_1 N_2}^{SRC,BB}$	$N_{N_1 N_2}^{BB}$	$N_{N_1 N_2}^{SRC,BB}$	$\mathcal{P}_{N_1 N_2}^{SRC,BB}$	$N_{N_1 N_2}^{BB}$	$N_{N_1 N_2}^{SRC,BB}$	$\mathcal{P}_{N_1 N_2}^{SRC,BB}$
pn	3.80	0.08	2.1	7.32	0.11	1.5	59.07	0.24	0.4
pp	1.72	0.01	0.6	3.27	0.01	0.4	27.61	0.02	0.1

TABLE II: The number of of back-to-back (BB) proton-neutron (pn) and proton-proton (pp) pairs (Eq.(27)) and the integrated momentum distribution of BB SRCd pairs (Eq.(28)) and the percent probability $\mathcal{P}_{N_1 N_2}^{SRC,BB} = 100 N_{N_1 N_2}^{SRC,BB} / N_{N_1 N_2}^{BB}$. Microscopic wave functions corresponding to the AV18 interaction [35], for ^2H and ^3He [32, 33], and to the AV8' interaction [36] for ^4He [34] and complex nuclei [15]. In brackets the values obtained with the VMC momentum distributions of Ref. [11], which are calculated with AV18+UX interaction.

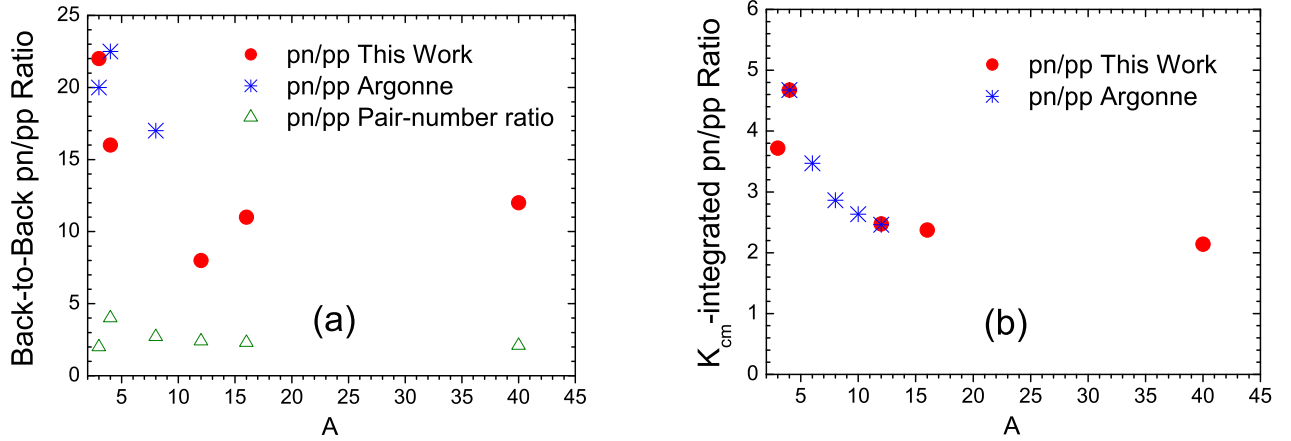


FIG. 14: (Color online) (a): The ratio $N_{pn}^{SRC,BB} / N_{pp}^{SRC,BB}$ using the wave functions of the present work (*cf.* Table II) and the VMC results of ref [11]. (b): the same as in (a) for the K_{cm} - integrated momentum distributions (*cf.* Table III).

(ST) values of the pair (mostly (10), (01), and (11)), contribute to the momentum distributions, as demonstrated in Refs. [7, 8], [17] and [11]. We will consider the following quantities: **1.** The total number of back-to-back $N_1 N_2$ pairs, $N_{N_1 N_2}^{BB}(K_{c.m.} = 0)$, resulting from the integration of the pair relative momentum and the total number of the *short-range correlated back-to-back* $N_1 N_2$ pairs, $N_{N_1 N_2}^{SRC,BB}(K_{c.m.} = 0, k_{rel} \geq 1.5)$, that are given, respectively by

$$\begin{aligned}
& N_{N_1 N_2}^{BB}(K_{c.m.} = 0) \\
&= 4 \pi \int_0^\infty n_A^{N_1 N_2}(k_{rel}, K_{c.m.} = 0) k_{rel}^2 dk_{rel} \\
&\equiv N_{N_1 N_2}^{BB}
\end{aligned} \tag{27}$$

$$\begin{aligned}
& N_{N_1 N_2}^{SRC,BB}(K_{c.m.} = 0, k_{rel} \geq 1.5) \\
&= 4 \pi \int_{1.5}^\infty n_A^{N_1 N_2}(k_{rel}, K_{c.m.} = 0) k_{rel}^2 dk_{rel} \\
&\equiv N_{N_1 N_2}^{SRC,BB}
\end{aligned} \tag{28}$$

In both Eqs. (27) and (28), whose values are shown in Table II, the quantity $n_A^{N_1 N_2}(k_{rel}, K_{c.m.} = 0)$ is the one shown in Figs. 1-5.⁸ It can be seen from Table II

⁸ Note that Eqs.(27) and (28) have the dimension of fm^3 provided by the c.m. momentum distribution at $K_{c.m.} = 0$. We call them anyway *number of particles for back-to-back pairs*.

	² H			³ He			⁴ He		
	$N_{N_1 N_2}$	N_D^{SRC}	$\mathcal{P}_D^{SRC}(\%)$	$N_{N_1 N_2}$	$N_{N_1 N_2}^{SRC}$	$\mathcal{P}_{N_1 N_2}^{SRC}(\%)$	$N_{N_1 N_2}$	$N_{N_1 N_2}^{SRC}$	$\mathcal{P}_{N_1 N_2}^{SRC}(\%)$
pn	1 (1)	0.036 (0.036)	3.6 (3.6)	2 –	0.093 –	4.7 –	4 –	0.243 (0.332)	6.1 (8.3)
pp	– –	– –	– –	1 –	0.025 –	2.5 –	1 –	0.052 (0.071)	5.2 (7.1)

	¹² C			¹⁶ O			⁴⁰ Ca		
	$N_{N_1 N_2}$	$N_{N_1 N_2}^{SRC}$	$\mathcal{P}_{N_1 N_2}^{SRC}(\%)$	$N_{N_1 N_2}$	$N_{N_1 N_2}^{SRC}$	$\mathcal{P}_{N_1 N_2}^{SRC}(\%)$	$N_{N_1 N_2}$	$N_{N_1 N_2}^{SRC}$	$\mathcal{P}_{N_1 N_2}^{SRC}(\%)$
pn	36 –	3.02 (3.74)	8.4 (10.4)	64 –	4.75 –	7.4 –	400 –	21.06 –	5.3 –
pp	15 –	1.22 (1.52)	8.1 (10.1)	28 –	2.00 –	7.1 –	190 –	9.86 –	5.2 –

TABLE III: The total number of pairs $N_{N_1 N_2}$ (Eq. 30), the total number of SRCd pairs $N_{N_1 N_2}^{SRC}$, Eq.(29) (in case of deuteron Eq.(26)) and their percent probability $\mathcal{P}_{N_1 N_2}^{SRC, BB} = 100 N_{N_1 N_2}^{SRC} / N_{N_1 N_2}$. Microscopic wave functions corresponding to the AV18 interaction [35] for ²H and ³He [32, 33] and the AV8' interaction [36] for ⁴He [34] and complex nuclei [15]. The values in brackets correspond to the VMC wave functions of Ref. [11].

	² H			³ He		
	$R_{pn}(\%)$	$R_{pp}(\%)$	$R_{pp/pn}$	$R_{pn}(\%)$	$R_{pp}(\%)$	$R_{pp/pn}$
THE	100	0	–	89.3	3.16	3.54
EXP	–	–	–	–	–	–

	⁴ He			¹² C		
	$R_{pn}(\%)$	$R_{pp}(\%)$	$R_{pp/pn}$	$R_{pn}(\%)$	$R_{pp}(\%)$	$R_{pp/pn}$
THE	93.2	5.43	5.83	96.2	5.01	5.20
EXP	87.0±14.1	3.9 ± 1.5	5.1 ± 2.6	97.0±22.1	4.8±1.0	5.8±1.5

	¹⁶ O			⁴⁰ Ca		
	$R_{pn}(\%)$	$R_{pp}(\%)$	$R_{pp/pn}$	$R_{pn}(\%)$	$R_{pp}(\%)$	$R_{pp/pn}$
THE	97.9	5.05	5.15	91.8	6.52	7.11
EXP	–	–	–	–	–	–

TABLE IV: The percent ratio of the pn and pp short-range correlated BB pairs with respect to the total number of correlated pairs and the percent ratio of pp to pn pairs (Eq. (31)) at $k_{rel} = 2.5 fm^{-1}$, calculated using the back-to-back momentum distributions shown in Figs. 1-5. Experimental data for ¹²C from Refs. [26–29] and for ⁴He from Ref. [30].

that for nuclei with $A > 4$ an appreciable decrease of the percent probabilities $\mathcal{P}_{N_1 N_2}^{SRC, BB}$ of back-to-back proton-neutron (pn) and proton-proton (pp) nucleons does occur with increasing values of A , which can be explained by the similar values of $n_A^{pn}(K_{c.m.} = 0)$ for $A \geq 12$ and, at the same time, the substantial increase of the value of the number of back-to-back proton-neutron and proton-proton nucleons $N_{N_1 N_2}^{BB}$ (Eq. (27));

2. The total number of SRCd pairs defined as the integral in the entire region of variation of $K_{c.m.}$ and in the region of the relative momentum with $k_{rel}^- \gtrsim 1.5 fm^{-1}$,

i.e.,

$$\begin{aligned}
N_{N_1 N_2}^{SRC}(k_{rel}^- = 1.5) &= \int_{1.5}^{\infty} d^3 k_{rel} \int_0^{\infty} d^3 K_{c.m.} n_A^{N_1 N_2}(\mathbf{k}_{rel}, \mathbf{K}_{c.m.}) \\
&= 4\pi \int_{1.5}^{\infty} k_{rel}^2 dk_{rel} n_A^{N_1 N_2}(k_{rel}) \equiv N_{N_1 N_2}^{SRC} \quad (29)
\end{aligned}$$

This quantity is compared with the total number of pairs given by

$$N_{N_1 N_2} = 4\pi \int_0^{\infty} k_{rel}^2 dk_{rel} n_A^{N_1 N_2}(k_{rel}) \quad (30)$$

The results are listed in Table III. The values of $N_{N_1 N_2}^{SRC}(k_{rel}^- = 1.5)$ include both two-nucleon SRCs (2NSRCs), as well as many-nucleon SRCs generated by the hard high-momentum tail ($K_{c.m.} \gtrsim 1$) of the c.m. distributions. Note, moreover, that the number of SRCd pairs is the largest one in this case since the entire variation of K_{cm} is taken into account; also worth being stressed is the almost constant value of the probability for $A \geq 12$ which is due to the same rate of increase of the number of correlated pairs and the total numbers of pN pairs N_{pN} . It can be seen from Fig. 11(b) that in the region $1.5 \lesssim k_{rel} \lesssim 3.5 \text{ fm}^{-1}$ the momentum components with $K_{c.m.} \neq 0$ are important in $n_A^{pn}(k_{rel})$. The main results of Table II and III are summarized in Fig. 14, whose main features should be stressed as follows:

1. because of the pn tensor dominance (see Figs. 1-5) the number of SRCd pn pairs in few-nucleon systems and $A < 12$ is larger than the number of pp pairs by about a factor twenty, whereas in medium-weight iso-scalar nuclei it is larger by about a factor ten, to be compared with a factor of two ($2Z/(Z-1)$), which is predicted by the naive pair-number ratio;
2. when the total, $K_{c.m.}$ -integrated number of pairs is considered, the value of the pn/pp ratio strongly decreases to a factor of about two, due to the role played by the c.m. high momentum components, as it can easily be understood by comparing Figs. 1(c)-2(c) with Figs. 1(d)-2(d) and Figs. 3(b)-5(b) with Figs. 3(c)-5(c).

VI. SHORT-RANGE CORRELATIONS: THEORETICAL PREDICTIONS VS EXPERIMENTAL DATA

Experimental investigation of SRCs is a complicated task mainly due to the small value of the involved cross sections and the effects of FSI that makes it difficult to reconstruct the initial correlated state. Nonetheless, experimental progress has been recently achieved thanks to the use of intense lepton beams and the development of advanced detector techniques. Nowadays it became possible to investigate quasi-elastic $A(e, e'N_1)X$ and $A(e, e'N_1N_2)X$ processes at high value of Q^2 and Bjorken scaling variable $x_B > 1$, a region where: (i) the contribution from non-nucleonic degrees of freedom is suppressed, (ii) the effects from initial-state SRCs are emphasized (see Ref.[1]-[5]), and (iii) the theoretical treatment of FSI has reached high degree of sophistication [19–22]. Several SRC properties that have been experimentally investigated deserve a comparison with theoretical calculations which is presented here-below.

A. The percent ratios of different kinds of N_1N_2 pairs in ^4He and ^{12}C and their missing momentum dependence

SRCs in ^4He and ^{12}C have been recently investigated [26–31] within the following kinematical region⁹: the squared four-momentum transfer $Q^2 \simeq 2 \text{ (GeV/c)}^2$, the bjorken scaling variable $x_{Bj} = 1.2$ and the three-momentum transfer $|\mathbf{q}| \equiv q \simeq 1.6 \text{ GeV/c}$. Information on the short-range momentum distribution of correlated pairs has been obtained by the following procedure: triple coincidence processes $^{12}\text{C}(p, p'pN)X$ and $^{12}\text{C}(e, e'pN)X$ have been performed by detecting, in coincidence with the struck, leading protons with high momentum \mathbf{p} , protons and neutrons moving with recoil momentum $\mathbf{p}_{rec} = \mathbf{q} - \mathbf{p}$ along a direction that, within the plane wave impulse approximation (PWIA), would coincide with the direction opposite to the momentum that the struck nucleon had before interaction with the projectile. Specifically, within the PWIA, if before interaction the struck proton had a momentum \mathbf{k}_1 , the leading proton would have a momentum $\mathbf{p} = \mathbf{k}_1 + \mathbf{q}$ and the known *missing momentum* would be $\mathbf{p}_m = \mathbf{q} - \mathbf{p} = -\mathbf{k}_1$. Therefore, if the struck proton "1" was partner of a correlated nucleon "2" with momentum $\mathbf{k}_2 \simeq -\mathbf{k}_1$, in coincidence with the leading proton a recoiling nucleon "2" with momentum $\mathbf{p}_{rec} = \mathbf{p}_m = -\mathbf{k}_1 \simeq \mathbf{k}_2$ should be observed along the direction opposite to \mathbf{p}_m . In Refs. [26–31] the processes $A(p, p'p)X$, $A(e, e'p)X$, $A(p, p'pp)X$, $A(e, e'pn)X$ and $A(e, e'pp)X$ have been investigated by detecting mainly back-to-back pp and pn nucleons in the range $1.5 \lesssim p_m \lesssim 3 \text{ fm}^{-1}$ in ^{12}C , and $1.5 \lesssim p_m \lesssim 4 \text{ fm}^{-1}$ in ^4He . Within such a kinematic set-up, the percent ratios of the cross sections pertaining to pn and pp pairs have been extracted. Using the two-nucleon relative momentum distributions shown in Figs. 1-5 corresponding to BB nucleons ($K_{c.m.} = 0$), we have calculated the following quantities:

$$\begin{aligned} R_{pn}(k_{rel}) &= \frac{n_A^{pn}}{n_A^p} \equiv \frac{pn}{p}; \\ R_{pp}(k_{rel}) &= \frac{n_A^{pp}}{n_A^p} \equiv \frac{pp}{p}; \\ R_{pp/pn}(k_{rel}) &= \frac{n_A^{pp}}{n_A^{pn}} \equiv \frac{pp}{pn} \end{aligned} \quad (31)$$

where $n_A^{pn} \equiv n_A^{pn}(k_{rel}, K_{c.m.} = 0)/n_{c.m.}^{pn}(K_{c.m.} = 0)$ and $n_A^{pp} \equiv n_A^{pp}(k_{rel}, K_{c.m.} = 0)/n_{c.m.}^{pp}(K_{c.m.} = 0)$. Here $n_A^{N_1 N_2}$ is related to the process $A(e, e'N_1N_2)X$ and n_A^p to the process $A(e, e'p)X$, which includes the contributions from pn and pp SRCs according to Eq. (19), therefore the ratios pn/p and pp/p represent essentially the percent ratios of the SRCd pp and pn pairs with respect to

⁹ The same notations as in Ref. [5] are adopted here

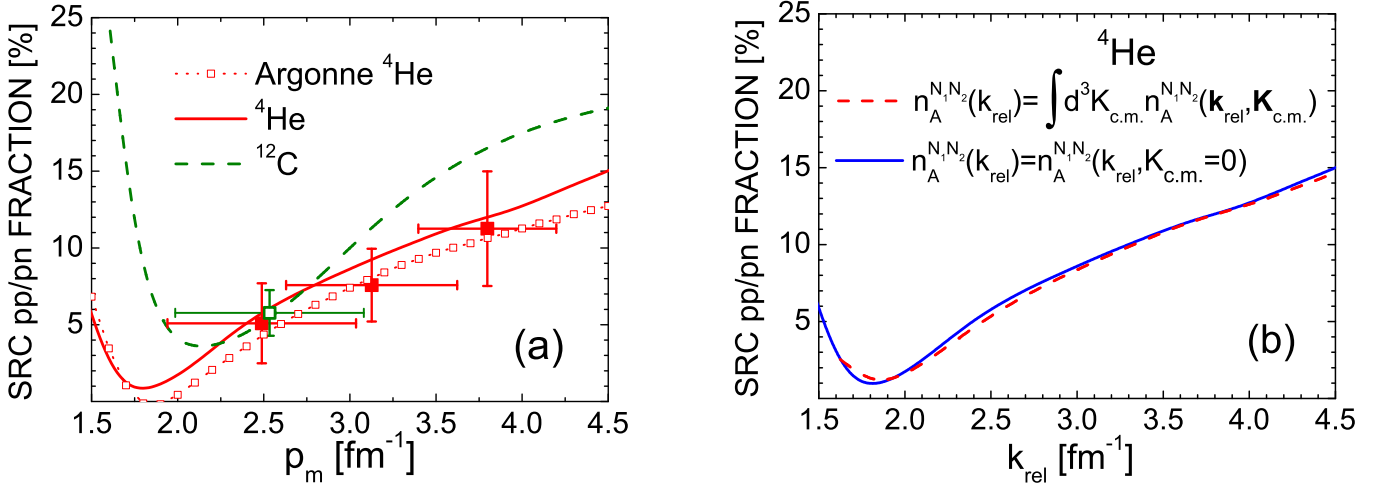


FIG. 15: (Color online) (a): the experimental percent of the pN BB pair fraction pp/pn , vs the missing momentum p_m , extracted from the processes $^4\text{He}(e, e'pn)X$ [30] and $^{12}\text{C}(e, e'pp)X$ [28, 29] compared with the quantity $R_{pp/pn}(k_{\text{rel}}, 0) = n_{pn}(k_{\text{rel}}, K_{\text{c.m.}} = 0)/n_{pp}(k_{\text{rel}}, K_{\text{c.m.}} = 0)$ calculated in the present paper (full line). The open squares show the results obtained with the Argonne momentum distributions [11]. (b): the same ratio as in (a) calculated within two different approaches: (i) full line: $n_{A=4}^{pn}(k_{\text{rel}}, K_{\text{c.m.}} = 0)/n_{A=4}^{pp}(k_{\text{rel}}, K_{\text{c.m.}} = 0)$; (ii) dashed line: $\frac{\int_0^\infty n_{pp}(k_{\text{rel}}, K_{\text{c.m.}}) K_{\text{c.m.}}^2 dK_{\text{c.m.}}}{\int_0^\infty n_{pn}(k_{\text{rel}}, K_{\text{c.m.}}) K_{\text{c.m.}}^2 dK_{\text{c.m.}}}$.

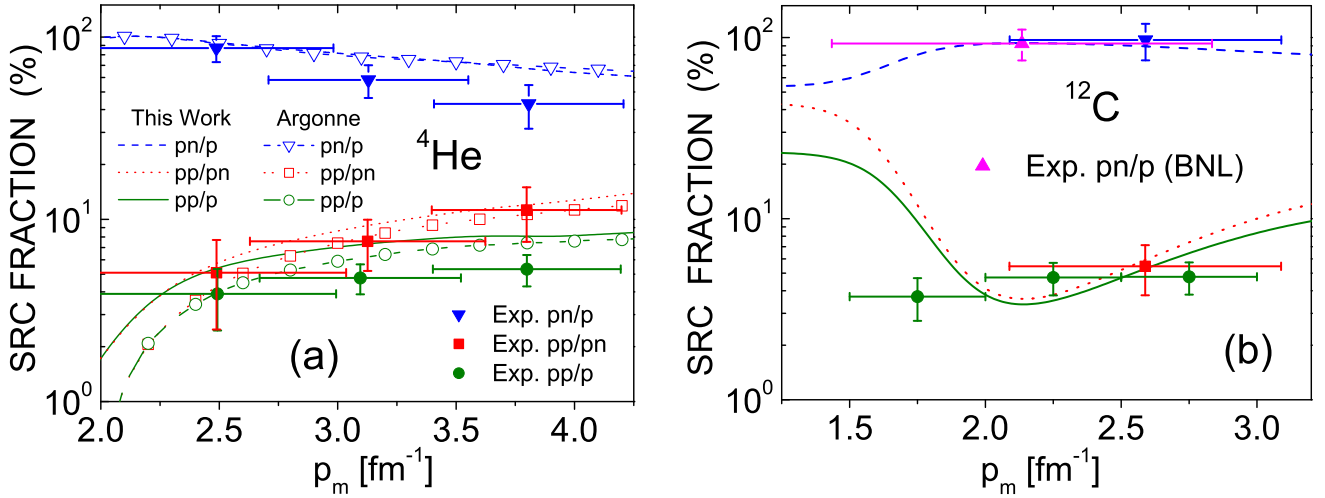


FIG. 16: (Color online) The experimental percent of SRC fractions in ^4He (a) and ^{12}C (b) compared with theoretical ratios of momentum distributions within the assumption $\mathbf{p}_m \simeq \mathbf{k}_{\text{rel}}$ and $K_{\text{c.m.}} = 0$. Momentum distributions from the present work and from Argonne VMC calculation [11]. All experimental data are from Jlab ([27]-[31]), except the one represented by the magenta point for ^{12}C that was obtained BNL [26]. In (b) the three theoretical curves have been obtained in the present work and correspond to pp/p (full), pn/p (dashed) and pp/pn (dot-dashed), respectively.

the total number of SRCd pairs. The quantities in Eq. (31) have been compared with the experimental data by assuming that $p_m \simeq k_{\text{rel}}$, a procedure that implies the

validity of the PWIA, or, at least, the cancellation of the FSI in the ratios. The comparison is presented in Table IV and in Figs. 15 and 16. A general agreement between

theoretical and experimental percent ratios appears to hold. Since the experiments have been performed in a momentum region where factorization of the wave functions is at work, the effects of the c.m. motion largely cancel out in the ratios. As for the effects of the FSI the experimental kinematics set-up is compatible with the assumption of FSI effects confined within the correlated pair, leading also in this case to some kind of cancelation in the ratio (see e.g. [2, 5, 19–22]). Concerning the results presented in these Figures the following comments are in order:

1. our results for ${}^4\text{He}$ do not practically differs from the ones obtained with the Argonne distributions;
2. in ${}^4\text{He}$ the increase with $p_m = |\mathbf{p}_m|$ of the pp/pn ratio can be explained with the increasing role of the repulsive NN interaction with respect to the tensor one (*cf* Fig. 2(c)); However, in spite of this satisfactory agreement, an advanced theoretical approach including FSI is desirable; preliminary results from Ref. [21, 22], quoted in [30] seem to correct the PWIA into the right direction;
3. the results presented in Fig. 15(b) show that the ratio calculated at $K_{c.m.} = 0$ or integrated by averaging over all direction of $\mathbf{K}_{c.m.}$ practically do not differ, which is another manifestation of factorization since the pp and pn c.m. momentum distributions are essentially the same.

B. The c.m. momentum distribution of correlated pairs in ${}^4\text{He}$ and ${}^{12}\text{C}$

The c.m. momentum distributions of a correlated pn pair relative to the spectator nucleus $A - 2$ in ${}^4\text{He}$ and pp pair in ${}^{12}\text{C}$ has been determined in Refs. [28] and [30] by analyzing the distribution of events in the process $A(e, e'pN)X$ as a function of the cosine of the opening angle γ between \mathbf{p}_m and \mathbf{p}_{rec} which, in PWIA, is the angle between \mathbf{k}_1 and \mathbf{k}_2 . The results of the analysis of the experimental data, corrected for the detector acceptance, are shown in Fig.17 where the theoretical momentum distributions are also shown. It turns out [41] that, once the theoretical curves are corrected taking into account the finite acceptance of the detectors they nicely agree with the experimental momentum distributions.

VII. SUMMARY AND CONCLUSIONS

In this paper we have investigated in-medium short-range nucleon-nucleon dynamics by calculating various kinds of two-nucleon momentum distribution in few-nucleon system and selected isoscalar nuclei with $A \leq 40$. To this end calculations have been performed within a parameter-free many-body approach which, even if not

fully *ab initio*, turned out to be capable to treat high momentum components in nuclei with $A \geq 12$, for which advanced VMC approaches with bare strongly repulsive local interactions, are unfortunately not yet feasible. The method, based upon a linked cluster expansion of one- and two-nucleon, diagonal and non-diagonal, density matrices, has been previously used to calculate the ground-state energy [15] and the momentum distributions [16, 17]. In this paper we have performed a detailed analysis of the two-nucleon momentum distributions $n_A^{N_1 N_2}(k_{rel}, K_{c.m.}, \Theta)$ at various values of k_{rel} , $K_{c.m.}$ and Θ , as well as of the two-nucleon relative, $n_A^{N_1 N_2}(k_{rel})$, and center-of-mass, $n_A^{N_1 N_2}(k_{c.m.})$, momentum distributions of proton-neutron and proton-proton pairs. The results of our calculations show that a fundamental property of the nuclear wave function at short inter-nucleon separations turns out to be its factorization into the relative and the c.m. coordinates, a property which has been previously theoretically illustrated in the case of nuclear matter [23] and few-nucleon systems [24]. Such a property is a very relevant one, for it fully governs the high momentum behavior of two-nucleon momentum distributions generated by short-range correlations. In particular, the following properties of in-medium two-nucleon dynamics, resulting from wave-function factorization, are worth being stressed:

1. in the region of relative distances $r_{ij} \gtrsim 1 - 1.5 \text{ fm}^{-1}$, nucleons "i" and "j" move independently in a mean field, with average relative momentum $k_{rel} \lesssim 1.5 - 2.0 \text{ fm}^{-1}$, without any particular difference between pp and pn distributions, apart from those due to the coulomb interaction; however, as soon as the relative distance decreases down to a value of $r_{ij} \lesssim 1 - 1.5 \text{ fm}^{-1}$, the two nucleons start feeling the details of the NN interaction, in particular the tensor force which makes the pn and pp motions to appreciably differ, with the difference decreasing at shorter distances, where the strong NN repulsive part of the local NN interaction dominates. In the SRC regions, characterized by a large content of high momentum components, thanks to the decoupling of the c.m. and the relative motions, also the two-nucleon momentum distribution, independently of the mass of the nucleus, factorizes into a relative and a c.m. parts; in particular, in the case of pn pairs one has $n_A^{pn}(k_{rel}, K_{c.m.}, \Theta) \simeq C_A^{pn} n_D^{pn}(k_{rel}) n_{c.m.}^{pn}(K_{c.m.})$, where C_A^{pn} is an A-dependent constant, the *nuclear contact*, which counts the number of deuteron-like pairs in nucleus A, and $n_D(k_{rel})$ is the deuteron momentum distribution; we have shown that the deuteron-like factorized form is valid only at low values of the c.m. momentum, $K_{c.m.} \lesssim 1 - 1.5 \text{ fm}^{-1}$ and, at the same time, at high values of the relative pair momentum $k_{rel} > k_{rel}^- \simeq 2 \text{ fm}^{-1}$, with the value of k_{rel}^- increasing with the value of K_{cm} ; thus, the dynamics of in-medium pn pairs can, to a large extent, be described as the dynamics of the motion in the nu-

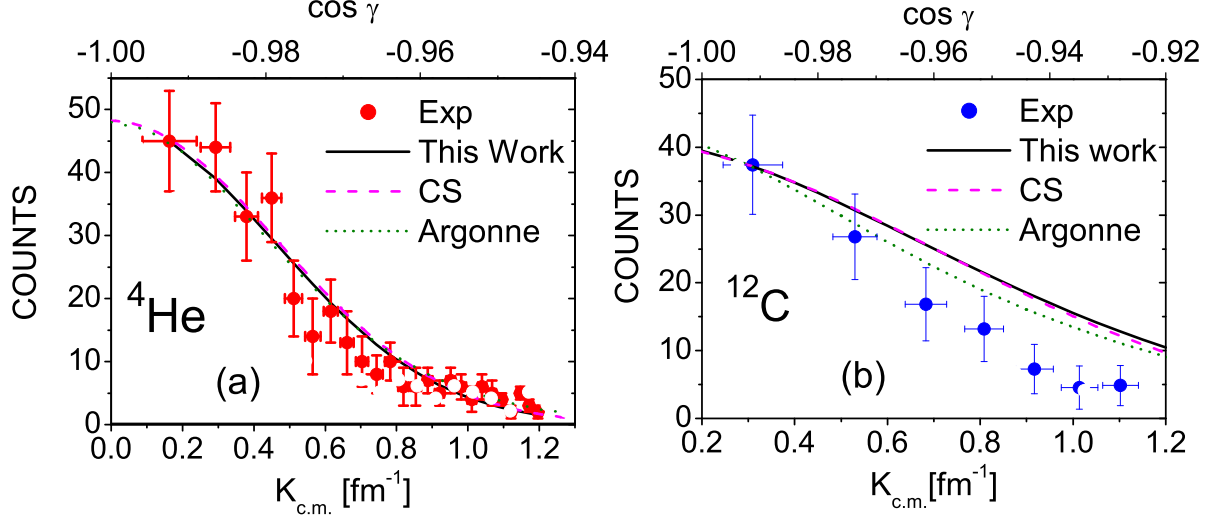


FIG. 17: (Color online) The c.m. momentum distribution of a pn pair in ^4He (a) and a pp pair in ^{12}C (b) extracted in Refs. [30] and [28] from the processes $^4\text{He}(e,e'pn)X$ and $^{12}\text{C}(e,e'pp)X$. γ is the angle between \mathbf{p}_m and \mathbf{p}_{rec} , which in PWIA is the angle between \mathbf{k}_1 and \mathbf{k}_2 . The values of $\mathbf{K}_{c.m.}$ have been obtained assuming $\mathbf{k}_2 = -\mathbf{k}_1$. The theoretical curves correspond to the momentum distributions of Ref. [11] (Argonne) and [25] (CS). The experimental data are given in arbitrary units and the theoretical calculations were normalized at the lowest available experimental point. Note that the discrepancy between the experimental data and the theoretical calculations in the case of ^{12}C is not a real one, since the latter, unlike the former, do not take into account the finite acceptance and resolution of the detectors [41]. Indeed, when these are taken into account, the data can be explained by a Gaussian distribution $n_{c.m.}(K_{c.m.}) = (\alpha/\pi)^{1.5} \exp(-\alpha K_{c.m.}^2)$ with $\alpha_{exp} = 0.97 \pm 0.19 \text{ fm}^2$ [28] in agreement with the three curves in Fig. 17(b).

cleus of a deuteron-like pair, whose c.m. moves with a momentum distribution $n_{c.m.}^{pn}(K_{c.m.})$;

2. within the above picture, arising from the factorization property of the momentum distributions, the ratio $n_A^{pn}(k_{rel}, K_{c.m.} = 0) / [n_D(k_{rel}) n_{c.m.}^{pn}(K_{c.m.} = 0)]$ at high relative values of k_{rel} should become a constant equal to C_A^{pn} , which is indeed the case; thus the theoretical values of the contacts C_A^{pn} , which have been determined by plotting the ratio *vs* k_{rel} , are completely free from any adjustable phenomenological parameter, for they are entirely defined in terms of many-body quantities that are fixed by the choice of the NN interaction and by the way the many-body problem is solved. This is true for all nuclei considered, both within our cluster expansion approach and the VMC *ab initio* calculation. The values of C_A^{pn} range from about 2 in ^3He to about 60 in ^{40}Ca ; for ^4He the value of C_A^{pn} is less by about 20% than the value obtained with the VMC momentum distribution; such a difference should be ascribed both to the different Hamiltonian (V8' NN interaction in our case and AV18 in Ref. [11]) and to the different variational wave functions; this point is under quantitative in-

vestigation;

3. for all nuclei that have been considered we found that when $k_{rel} \gtrsim 2 \text{ fm}^{-1}$, the ratio $n_A^{pn}(k_{rel}, K_{c.m.} = 0) / [C_A^{pn} n_{c.m.}^{pn}(K_{c.m.})]$ practically does not differ from the deuteron momentum distribution $n_D(k_{rel})$, which is a further clear evidence of factorization of $n_A^{pn}(k_{rel}, K_{c.m.}, \Theta)$; factorization also occurs when the numerator of the ratio is replaced by the $K_{c.m.}$ -integrated momentum distribution $n_A^{pn}(k_{rel})$, obtaining the ratio $n_A^{pn}(k_{rel}) / [C_A^{pn} n_{c.m.}^{pn}(K_{c.m.})]$; this however is only true at very high values of $k_{rel} \gtrsim 4 \text{ fm}^{-1}$; this means that at $k_{rel} \gtrsim 4 \text{ fm}^{-1}$ $n_A^{pn}(k_{rel})$ is dominated by the deuteron-like components with $K_{c.m.} = 0$, whereas at lower values of $K_{c.m.}$ also the c.m. components with $K_{c.m.} \neq 0$ contribute;
4. we have considered the relationships between the one-nucleon and the two-nucleon momentum distribution, a topic recently discussed in Ref. [39]. To this end we have compared three different approaches, namely: (i) the one in which only back-to-back ($K_{c.m.} = 0$) correlated nucleons are considered; (ii) the convolution model developed in

Ref. [25]; (iii) the approach of Ref. [39], where the two-nucleon momentum distributions are considered in the asymptotic limit $k_1 \gg K_{c.m.}$; our results demonstrate that in all of the three approaches the one-nucleon momentum distribution can be expressed, to a large extent, in terms of a proper sum of the pn and pp distributions, starting from a value of the one-nucleon momentum $k_1 \gtrsim 2 fm^{-1}$, within approaches (i) and (ii) and starting at $k_1 \gtrsim 4 fm^{-1}$, within approach (iii) ;

5. the two-nucleon momentum distributions have been used to calculate the absolute values of the number of SRCd pn and pp pairs in the considered nuclei; in particular we have calculated the number of BB SRCd pairs, defined by the integral of the two-nucleon momentum distribution in correspondence of $K_{c.m.} = 0$ and (similar to the deuteron case) in the relative momentum range $1.5 < k_{rel} < \infty fm^{-1}$, finding in complex nuclei a number of BB SRCd pn pairs larger than the number of pp pairs by about a factor of 10; concerning the numbers of SRCd nucleons it should be stressed that that in our approach the one- and two-nucleon momentum distribution satisfy the exact relationship provided by Eq.(19), which is valid in the entire region of momentum $0 < k_1 < \infty fm^{-1}$, so that the obtained two-nucleon momentum distributions provide a percent ratio of SRCd nucleons to the total number of nucleons in the range of 16-20 %, if SRCs are defined with respect to a pure independent-particle shell-model description.
6. The dependence upon k_{rel} and $K_{c.m.}$ of the two-nucleon momentum distributions of 4He and ^{12}C in the region of SRCs is in good agreement with available experimental data [26–31], and so are the c.m. distributions.

Several aspects of the above picture, which we have shown to occur also in light nuclei ($A \leq 12$) treated

within the VMC approach [11], have already been experimentally confirmed, whereas some others, concerning in particular the values of the nuclear contact in various spin-isospin states, deserve further theoretical and experimental investigations. Finally, we would like to stress that our approach provides momentum distributions that in some momentum regions are lower by 15-20 % than the ones calculated with the VMC momentum distributions; as already pointed out, this can be attributed partly to the different Hamiltonian used in the two approaches, and partly to the different variational wave functions; this point is under investigation. To conclude, our approach turned out to be accurate enough to describe the main features of SRCs in few-nucleon systems and iso-scalar nuclei with $A \leq 40$, so that it should deserve the extension to different types of NN interaction models differing, particularly, in the short range behavior, and should be applied to heavier neutron-rich nuclei, whose investigation presents several interesting aspects [31, 43].

VIII. ACKNOWLEDGMENTS

This work has been performed within the activity and support of the Theory Group of the Italian Istituto Nazionale di Fisica Nucleare (INFN), Sezione Perugia. H. M. is grateful to INFN for kind hospitality and support. We gratefully acknowledge Robert Wiringa for providing useful information about the effects of the 3N force on the high momentum components, within the VMC approach. M.A. acknowledges the CINECA award under the ISCRA initiative, for the availability of high performance computing resources.

-
- [1] L. Frankfurt, M. Sargsian and M. Strikman, Int. J. Mod. Phys. A **23**, 2991 (2008)
 - [2] J. Arrington, D. W. Higinbotham, G. Rosner and M. Sargsian, Prog. Part. Nucl. Phys. **67**, 898 (2012)
 - [3] M. Alvioli, C. Ciofi degli Atti, L. P. Kaptari, C. B. Mezzetti and H. Morita, Int. J. Mod. Phys. E **22**, 1330021 (2013)
 - [4] C. Ciofi degli Atti, *Realistic NN interactions and two-nucleon dynamics in nuclear medium*. Chapter of the Book: *NN and 3N Interactions*, Nova Science Pub. Inc., New York, 2014
 - [5] C. Ciofi degli Atti, Phys. Rept. **590**, 1 (2015).
 - [6] Y. Suzuki and W. Horiuchi, Nucl. Phys. A **818**, 188 (2009)
 - [7] H. Feldmeier, W. Horiuchi, T. Neff and Y. Suzuki, Phys. Rev. C **84**, 054003 (2011);
 - [8] R. Roth, T. Neff and H. Feldmeier, Prog. Part. Nucl. Phys. **65**, 50 (2010)
 - [9] R. Schiavilla, R. B. Wiringa, S. C. Pieper and J. Carlson, Phys. Rev. Lett. **98**, 132501 (2007)
 - [10] M. Alvioli, C. Ciofi degli Atti, L. P. Kaptari, C. B. Mezzetti, H. Morita and S. Scopetta, Phys. Rev. C **85**, 021001 (2012)
 - [11] R. B. Wiringa, R. Schiavilla, S. C. Pieper and J. Carlson, Phys. Rev. C **89** 024305 (2014).
 - [12] M. Gaudin, J. Gillespie and G. Ripka, Nucl. Phys. A **176**, 237 (1971).
 - [13] O. Bohigas and S. Stringari, Phys. Lett. B **95**, 9 (1980).
 - [14] F. Arias de Saavedra, C. Bisconti, G. Co' and A. Fabrocini, Phys. Rept. **450**, 1 (2007)
 - [15] M. Alvioli, C. Ciofi degli Atti and H. Morita, Phys. Rev. C **72**, 054310 (2005)

- [16] M. Alvioli, C. Ciofi degli Atti and H. Morita, Phys. Rev. Lett. **100**, 162503 (2008).
- [17] M. Alvioli, C. Ciofi degli Atti, L. P. Kaptari, C. B. Mezzetti and H. Morita, Phys. Rev. C **87** 034603 (2013).
- [18] L. L. Frankfurt and M. I. Strikman, Phys. Rept. **160**, 235 (1988).
- [19] L. L. Frankfurt, M. M. Sargsian and M. I. Strikman, Phys. Rev. C **56**, 1124 (1997)
- [20] I. Mardor, Y. Mardor, E. Piasetzky, J. Alster and M. M. Sargsian, Phys. Rev. C **46**, 761 (1992). C. Ciofi degli Atti and L. P. Kaptari, Phys. Rev. Lett. **100**, 122301 (2008)
- [21] J. Ryckebusch, D. Debruyne, P. Lava, S. Janssen, B. Van Overmeire and T. Van Cauteren, Nucl. Phys. A **728**, 226 (2003)
- [22] W. Cosyn, M. C. Martinez and J. Ryckebusch, Phys. Rev. C **77**, 034602 (2008)
- [23] M. Baldo, M. Borromeo and C. Ciofi degli Atti, Nucl. Phys. A **604**, 429 (1996).
- [24] C. Ciofi degli Atti, L. P. Kaptari, S. Scopetta and H. Morita, Few Body Syst. **50**, 243 (2011)
- [25] C. Ciofi degli Atti and S. Simula, Phys. Rev. C **53**, 1689 (1996)
- [26] A. Tang *et al.*, Phys. Rev. Lett. **90**, 042301 (2003)
- [27] E. Piasetzky, M. Sargsian, L. Frankfurt, M. Strikman and J. W. Watson, Phys. Rev. Lett. **97**, 162504 (2006)
- [28] R. Shneor *et al.* [Jefferson Lab Hall A Collaboration], Phys. Rev. Lett. **99**, 072501 (2007)
- [29] R. Subedi *et al.*, Science **320**, 1476 (2008)
- [30] I. Korover *et al.* [Lab Hall A Collaboration], Phys. Rev. Lett. **113**022501 (2014).
- [31] O. Hen *et al.*, Science **346**, 614 (2014)
- [32] A. Kievsky, S. Rosati and M. Viviani, Nucl. Phys. A **551**, 241 (1993).
- [33] A. Kievsky, M. Viviani, L. Girlanda and L. E. Marcucci, Phys. Rev. C **81**, 044003 (2010)
- [34] H. Morita, unpublished.
- [35] R. B. Wiringa, V. G. J. Stoks and R. Schiavilla, Phys. Rev. C **51**, 38 (1995)
- [36] B. S. Pudliner, V. R. Pandharipande, J. Carlson, S. C. Pieper and R. B. Wiringa, Phys. Rev. C **56**, 1720 (1997)
- [37] R. B. Wiringa, *Private communication*.
- [38] S. Tan, Ann. Phys. **323** 2952-2990 (2008).
- [39] R. Weiss, B. Bazak and N. Barnea, Phys. Rev. C **92** 054311 (2015)
- [40] O. Hen, L. B. Weinstein, E. Piasetzky, G. A. Miller, M. M. Sargsian and Y. Sagi, Phys. Rev. C **92** 045205 (2015)
- [41] O. Hen, E. Piasetzky, *Private Communication*.
- [42] R. Schiavilla, V. R. Pandharipande and R. B. Wiringa, Nucl. Phys. A **449**, 219 (1986).
- [43] M. M. Sargsian, Phys. Rev. C **89** 034305 (2014).

